RAMAN SPECTRA OF VAN DER WAALS COMPLEXES IN ARGON

Clifford Eugene Morgan, et al

Texas University

Prepared for:

Air Force Office of Scientific Research

12 January 1973

Raman Spectra of Van der Waals Complexes in Argon

by

Clifford Eugene Morgan and L. Frommhold
Department of Physics

Technical Report No: 142
January 12, 1973

PLASMA AND QUANTUM ELECTRONICS RESEARCH LABORTORY

ELECTRONICS RESEARCH CENTER
THE UNIVERSITY OF TEXAS AT AUSTIN
Austin, Texas 78712

The Electronics Research Center at The University of Texas at Austin constitutes interdisciplinary laboratories in which graduate faculty members and graduate candidates from numerous academic disciplines conduct research.

Research conducted for this technical report was supported in part by the Department of Defense's JOINT SERVICES ELECTRONICS PROGRAM (U.S. Army, U.S. Navy, and the U.S. Air Force) through the Research Contract AFOSR F44620-71-C-0091. This program is monitored by the Department of Defense's JSEP Technical Advisory Committee consisting of representatives from the U.S. Army Electronics Command, U.S. Army Research Office, Office of Naval Research, and the U.S. Air Force Office of Scientific Research.

Additional support of specific projects by other Federal Agencies, Foundations, and The University of Texas at Austin is acknowledged in footnotes to the appropriate sections.

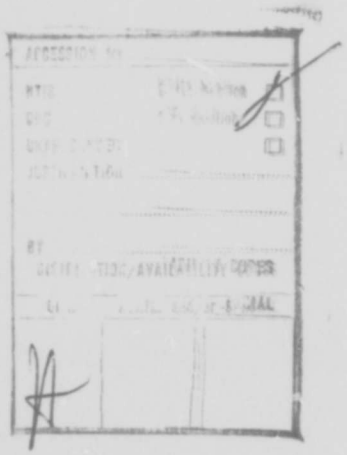

UNCLASSIFIED

Security Classification

DOCUMENT CONTROL DATA - R & D

(Security classification of title, body of abstract and indexing annotation must be entered when the overall report is classified)

1. ORIGINATING ACTIVITY (Corporate author) The University of Texas at Austin Electronics Research Center Austin, Texas 78712	2a. REPORT SECURITY CLASSIFICATION Unclassified 2b. GROUP

3. REPORT TITLE

RAMAN SPECTRA OF VAN DER WAALS COMPLEXES IN ARGON

4. DESCRIPTIVE NOTES (Type of report and inclusive dates)

Scientific ---------- Interim

5. AUTHOR(S) (First name, middle initial, last name)

Clifford Eugene Morgan and L. Frommhold

6. REPORT DATE 12 January 1973	7a. TOTAL NO. OF PAGES 127	7b. NO. OF REFS 54
8a. CONTRACT OR GRANT NO b. PROJECT NO. c. d.	F44620-71-C-0091 4751 61102F 681305	9a. ORIGINATOR'S REPORT NUMBER(S) TR-142 9b. OTHER REPORT NO(S) (Any other numbers that may be assigned this report) AFOSR - TR - 73 - 0561

10. DISTRIBUTION STATEMENT

Approved for public release; distribution unlimited

11. SUPPLEMENTARY NOTES TECH, OTHER.	12. SPONSORING MILITARY ACTIVITY JSEP through AF Office of Scientific Research (NE) 1400 Wilson Blvd., Arlington, VA 22209

13. ABSTRACT

The Raman spectra of high purity helium, xenon, and especially argon, were observed at a number of temperatures between the boiling points and 300°K and pressures from vacuum to four atmospheres. Because of the high sensitivity of the experiment, the spectra were obtained at gas densities for which predominantly two-body collisions occurred and at gas temperatures widely different from room temperature, in contrast to previous work in this field. The intensity of the scattered light varies as the square of the gas density indicating a diatomic process. The slope of the logarithm of the logarithm of the scattered intensity versus the frequency shift varies as the inverse absolute temperature. In addition, the scattering is completely depolarized and the ratio of the Stokes intensity to the anti-Stokes intensity is equal to a Boltzmann factor.

In the spectra of argon, a continuous band structure resembling an unresolved pure rotation band was observed. The wavelength, corresponding to the peak of the band structure, shifts with temperature in agreement with the theoretical shifts for a pure rotation band of a diatomic molecule. The value of the rotational constant is in good agreement with that determined for the atomic mass of argon and Van der Waals radii calculated from second virial coefficient data for argon.

A similar band structure was observed for xenon, but with peaks evidently so close to the Rayleigh line that only shoulders were resolved. Again the shoulders shifted inward with decreasing temperature in agreement with the expected behavior of a pure rotation band. The rotational constant, derived from the data, is in good agreement with that expected for a xenon dimer.

In the case of helium, only slight scattering was observed at the lowest temperature and highest pressure. It was, therefore, impossible to study the parameter dependence of this scattering.

These new results do not completely agree with present theories of light scattering by noble gases. It is suggested that the light scattering is due to a metastable Van der Waals dimer or complex. The dependence of the scattered intensity on gas density and temperature is in excellent agreement with that predicted for Van der Waals dimers.

DD FORM 1 NOV 68 1473

UNCLASSIFIED

Security Classification

KEY WORDS	ROLE	WT	ROLE	WT	ROLE	WT
RAMAN SPECTROSCOPY						
VAN-DER-WAALS MOLECULES						
LASER RAMAN SPECTROSCOPY						

RAMAN SPECTRA OF VAN DER WAALS COMPLEXES IN ARGON*

by

Clifford Eugene Morgan and L. Frommhold
Department of Physics

Technical Report No. 142
January 12, 1973

PLASMA AND QUANTUM RESEARCH LABORATORY

ELECTRONICS RESEARCH CENTER
THE UNIVERSITY OF TEXAS AT AUSTIN
Austin, Texas 78712

*Research sponsored by the Joint Services Electronics Program under Research Contract F44620-71-C-0091.

TABLE OF CONTENTS

LIST OF FIGURES

CHAPTER I

INTRODUCTION

The process of condensation of a gas to a liquid has long been of great interest to both physicists and chemists, and, although much work has been done, understanding of the process is far from complete. The role of van der Waals forces in condensation undoubtedly is important. In particular, it has been suspected for some time that, as a consequence of the van der Waals forces, a kind of molecule can be formed even from atoms of the noble gases. Such molecules are called van der Waals molecules.

Molecules may be classified according to their stability as chemically stable and physically stable molecules. Chemically stable molecules have lifetimes very much greater than the time between collisions in the gas; while physically stable molecules have lifetimes that are greater than the duration time of a collision, but less than a time which is somewhat longer than the time between collisions.

Van der Waals molecules fall into the latter category. Two further types of van der Waals molecules

may be distinguished: metastable molecules which can dissociate spontaneously and stable molecules which dissociate only on collision. In the remainder of this work, a van der Waals molecule consisting of two atoms or two chemically stable molecules will be called a van der Waals dimer or simply a dimer.

If two atoms are associated for a length of time the same as, or less than, the duration of a collision they are called collision pairs. Collision pairs are usually not considered in any sense to be bound molecules since their behaviour is generally distinctly different from that of molecules, whether physically stable or chemically stable.

It is evident that the ability of two or more atoms to remain in a region of space relatively close to each other for a time appreciably longer than the time required for mere transit of this region is the fundamental distinguishing characteristic of a molecule.

Spectroscopic methods have long been among the most accurate techniques for determining the properties of molecules. In particular, it is an experimental fact that Raman spectroscopy is a useful means of investigating the properties of highly symmetrical, nonpolar molecules.

Inasmuch as the van der Waals dimers of a pure monoatomic gas are necessarily homonuclear, diatomic, and nonpolar, Raman spectroscopy is definitely applicable to their study. If visible light is used to excite the Raman spectrum, it is necessary that the sample gas have molecular states, otherwise no Raman spectrum could be observed. As a consequence of the fact that the pure noble gases do not form chemically stable molecules, Raman scattering can only arise from collision pairs or van der Waals molecules in the noble gases. A particularly simple and easily interpreted experimental situation thus obtains, and, therefore, the Raman spectra of helium, argon, and xenon were investigated. The Raman spectrum of helium was too weak for study and the quantity of xenon necessary for extensive study was too expensive; hence, the principal subject of this dissertation is the Raman spectrum of argon.

C H A P T E R I I

HISTORICAL BACKGROUND

Following the discovery of the noble gases in the last decade of the nineteenth century, many attempts were made to obtain chemical reaction with them (see Reference 1 for a review). Practically all of these attempts led to negative results, and by 1916 it had been established that the noble gases were chemically inert and the theory of chemical binding had confirmed this result. However, the possibility of the occurrence of physically stable molecules in noble gases had not been precluded. Indeed, Jeans (Reference 2) in 1904 had anticipated the existence of aggregates of molecules in gases on the basis of the small attractive van der Waals force, known from the non-ideal behaviour of real gases. Later, Frenkel (Reference 3) refered more specifically to the existence of dimers. The first important theoretical work on dimers, however, appears to have been that by Stogryn and Hirschfelder (References 4 and 5). Using square-well, Sutherland, and Lennard-Jones (6-12) interaction potentials between the monomers, they calculated the contributions to the

second virial coefficient by collision pairs, physically stable dimers, and metastable dimers in a gas. They also calculated the mean lifetimes of metastable dimers in argon and obtained values between 10^{-11} second and about 10^{16} seconds. An equation for the maximum number of vibrational levels was obtained also. At temperatures less than the critical temperature, the dimers give the major contribution to the second virial coefficient, and at temperatures below the Boyle temperature the dimer contribution is still significant.

The first direct experimental evidence for the formation of dimers appears to have been the work of Vu and Vodar (Reference 6). These workers studied the region of the fundamental band in the infrared of mixtures of hydrogen chloride with argon and with nitrogen. At low temperatures and high pressures, they observed that, as the density of argon or nitrogen was increased, the vibration-rotation band progressively transformed into a pure vibration band, shifted in frequency. On the other hand, if the density was held constant and the temperature increased, the inverse transformation occurred. The results were interpreted in terms of orbiting dimers consisting of an hydrogen chloride molecule plus an argon atom or plus a nitrogen molecule.

A few years later Watanabe and Welsh (Reference 7) obtained experimental evidence for dimers in the pressure-induced infrared absorption of molecular hydrogen at 20°K. Two physically stable (J = 0, 1) and two metastable (J = 2, 3) species of dimers were found with intermolecular distances in the range 4.2 to 4.6 Å. (J is the quantum number for angular momentum.) The average term values of the vibrational states of the dimers were v_0 = 0, v_1 = 1.9, v_2 = 4.8, and v_3 = 9.1 cm^{-1}. They calculated that about 0.1% of the hydrogen molecules were in dimer states.

The first strong experimental evidence for dimers of neutral, unexcited noble-gas atoms was obtained in 1965 by Leckenby and Robbins (Reference 8, 9, 10). A mass spectrometer was used to measure the concentrations of dimers in argon, xenon, CO_2, N_2O, N_2, O_2 and H_2O. The dimer concentration in argon was found to vary linearly with gas pressure over a range of from about 50 to 300 torr at room temperature. Above one atmosphere of argon pressure, the dimer concentration was stated to rise more rapidly with pressure. When allowance was made for the loss of metastable dimers due to spontaneous dissociation, the variation of dimer concentration with temperature over

the range of from 180°K to 300°K for both argon and xenon was found to agree approximately with a $T^{-5/2}$ law, where T is the absolute temperature of the gas. The concentration of xenon dimers at a given temperature and pressure was found to be much greater than argon dimers. Leckenby and Robbins concluded that dimers exist in all gases at temperatures at which the attractive van der Waals force is important and at pressures high enough to produce a significant fraction of three-body collisions.

After these initial discoveries, a series of investigations were made leading up to the work on light scattering by noble gases.

Welsh et al. (References 11, 12, 13, 14) extended their pressure-induced infrared absorption investigations to other gases and gas mixtures, finding evidence for $(D_2)_2$, H_2-A_r, H_2-N_2, H_2-K_r, and H_2-Xe dimers, but no evidence for dimer formation in H_2-He mixtures.

Ogryzlo and Sanctuary (Reference 15) observed evidence for the formation of dimers in bromine vapor in the ultraviolet absorption region between 1850 and 2500 Å. The absorbance varied as the square of the bromine concentration and increased with decreasing temperature.

Milne and Green (Reference 16) studied nucleation phenomena in nozzle beams with a mass spectrometer. The

gases became highly supersaturated after expanding through the nozzle and clusters of up to 45 atoms were observed in argon. It was also found that addition of a few percent of CO_2 or D_2O to pure argon drastically reduced the number of argon dimers observed. Once again, the lifetimes of the metastable dimers were probably too short to be detected by the apparatus. The measured pressure dependence of the concentration of dimers agreed with the theoretical predictions of Stogryn and Hirschfelder.

Apparently, the first observations of the Raman spectra of noble gases were made by McTague and Birnbaum (Reference 17 and 18). Argon, krypton, and xenon were investigated at room temperature and at densities from about 30 amagats to about 150 amagats. For each gas, a broad continuum was observed starting from the wings of the Rayleigh line at about 6 cm^{-1}, extending to 50 cm^{-1}, and exhibiting a simple exponential shape devoid of peaks and valleys. In addition, the scattering was depolarized and the intensity varied with the square of the gas density, except at the higher densities investigated. At higher densities departure from the square law was observed with the appearance of a cubic density term having a negative coefficient. They attributed this scattering to collision pairs in the gases.

In the meantime, a theory had been developed by Levine and Birnbaum (Reference 19) to explain light scattering that arises from distortion of the electronic structure of two molecules during collision. This theory predicted that, for binary collisions, light is scattered into a broad frequency band, the width of which is determined by the duration of a collision and the intensity of which varies as the square of the density. The collision-induced polarizability was assumed to have a Gaussian dependence on intermolecular separation. The derived expressions agree with most of the findings of McTague and Birnbaum, and result in a spectrum which has its maximum value at zero frequency shift and which monotonically decreases with increasing frequency shift in a symmetrical manner about the zero frequency shift.

In the year 1968, Shardanand (Reference 20 and 21) observed the photoattenuation cross section of xenon and found that it did not follow Beer's law, but instead exhibited a linear increase with gas pressure and a decrease (as T^{-1}) with gas temperature. The presence of Xe_2 molecules was deduced from this behaviour and the heat of dissociation)0.03 ± 0.001 ev) and equilibrium constant for formation of dimers (2.16×10^{-22} cm^3/molecule)

derived. In fact, however, these results are just as valid for collision pairs as stable molecules and are no more evidence for the existence of bound molecules than for the existence of collision pairs in the gas.

In 1969, Tanaka and Yoshino (Reference 22) observed the absorption spectrum of the He_2 molecule in the vacuum ultraviolet. Transitions were observed between the states $A\ ^1\Sigma_u^+$ and $X\ ^1\Sigma_g^+$, the upper state being a bound state and the lower state a repulsive one. The spectrum is due to the reverse of the process that gives rise to the emission bands observed by a number of workers (References 23, 24, 25, and 26). The He_2 molecule does not, therefore, consist of two ground state helium atoms.

In 1970, Tanaka and Yoshino (Reference 27) reported the observation of the absorption spectrum of Ar_2 in the vacuum ultraviolet region. They identified nine discrete band systems and argue on the basis of an analogy with an earlier study of the emission continuum of the xenon molecule (References 28 and 29) that the ground state is stable. For the ground state, a dissociation energy of 76.9 cm^{-1} and six vibrational levels v = 0 - 5 are determined from the data. The spacing of the vibrational levels is given by

$$\omega_e = 30.68 \pm 0.37 \text{ cm}^{-1}$$

and

$$\omega_e x_e = 2.56 \pm 0.12 \text{ cm}^{-1}$$

During observations, the sample cell was cooled to liquid nitrogen temperature. At pressures less than .01 torr, the spectrum consisted entirely of sharp atomic lines which were broadened with increase of pressure; at 0.7 torr, additional features appeared which are appropriate to molecular bands; at 2.0 torr, forbidden lines of atomic argon appeared; and, at 30 torr or greater, the entire absorption spectrum becomes nearly a continuum. They were unable, however, to determine the rotational constant of ground state Ar_2. Also, no reliable evidence for metastable dimers could be found. Unfortunately, the temperature and density dependences were not investigated, so that there is some room to doubt that the results were not obtained from absorption by impurities in the gas.

Finally, refinements to the theory of collision-induced light scattering in noble gases were provided by Gersten (References 30 and 31) and Lewis and van Kranendonk (Reference 32) in the period 1970 to 1971. The chief

improvement by Gersten is the use of more realistic interatomic potentials. Lewis and van Kranendonk discussed interference effects in collision-induced scattering of noble gases and showed that they lead to a spectrum with a peak at the incident frequency and a width proportional to the gas density. Gersten, Slusher, and Surko (Reference 30) reported new data on Raman spectra of argon and krypton at 300 °K and 50 to 100 atmospheres. A broad, depolarized continuum was again observed, the shape of which could be approximated by a series of different exponentials one for each range of frequency shift. The results were attributed to scattering by collision pairs.

These previous investigations give strong evidence for the existence of ground state van der Waals dimers in the noble gases (except helium). In most of the experiments, either the temperature or the density dependence or both were not investigated. The temperature dependence of the Raman scattering of argon, krypton, and xenon was not determined and the vacuum ultraviolet spectroscopic investigations evidently did not determine the density or the temperature dependence of the observed absorption. Hence, there is room for reasonable doubts about the source of the observed spectra. The Raman

spectra were taken at such high densities that dimers, with their large interatomic separation distance, would surely be perturbed by nearly atoms. In no instance was the rotational constant for dimers in the noble gases determined. Finally, metastable dimers, although predicted by theory, were not observed in the noble gases by any previous workers.

C H A P T E R I I I

THEORY

The theory of Rayleigh and Raman scattering has been discussed in complete detail by Placzek (Reference 33). Reference also should be made to Anderson (Reference 34) for a modern quantum electrodynamic treatment of the theory. The theory of Raman scattering per se, therefore, will not be discussed in this work. Instead, the various mechanisms which have been proposed to explain light scattering by monoatomic gases will be succinctly discussed.

Conceivably, three sources could give rise to light scattering by monoatomic gases: scattering from the isolated atoms, scattering from collision pairs, and scattering from van der Waals molecules. Scattering by isolated atoms (i.e., noninteracting atoms) gives rise to a Rayleigh line with a Doppler-broadened profile characteristic of the velocity distribution of the atoms. In case an acoustic wave can be induced by the incident light, it is possible to observe Brillouin scattering from the gas (Reference 35). The peaks due to Brillouin scattering and the Doppler broadening are never more than a few tenths

of a wavenumber from the Rayleigh line at the temperatures and pressures used in this experiment and, therefore, this source of light scattering is not of any great importance for understanding the results of this investigation. Only the remaining two sources will be discussed further.

Scattering by collision pairs has been approached from two directions: namely, from consideration of fluctuations (due to nearby atoms) of the effective polarizing field (due to the incident light) experienced by a given atom (see, for example, Reference 36) and from consideration of the polarizability of collision pairs as compared with that of the isolated atoms (Reference 19). The main result of the first approach is that the Rayleigh scattering is not completely polarized even in the case of isotropic atoms. Also, the scattered intensity is predicted to vary in first order according to the sum of two terms: one proportional to the first power of the gas density and the square of the atomic polarizability, and the other proportional to the square of the density and the cube of the atomic polarizability. This type of scattering is not expected to be observable until the gas density is larger than 10 amagats. The second approach yields a

light scattering characterized by a broad continuum of large bandwidth determined by the duration of a collision. For binary collisions, the scattered intensity varies as the square of the gas density and, falls off in the wings as

$$f(T)\ \exp(-\text{ constant } x|\Delta\nu|(m/kT)^{1/2})$$

where $\Delta\nu$ is the frequency shift, m is the reduced mass of the collision pairs, k is Boltzmann's constant, and T is absolute temperature. f(T) contains terms which vary as T^{-1}, $T^{-3/2}$, and T^{-2}. In addition, the depolarization ratio of the scattering increases linearly with frequency shift from about 0.05 to about 0.06 on going from 0 to 30 cm^{-1} frequency shift. (Here completely depolarized light has a depolarization ratio of 0.75.) The maximum scattered intensity occurs at zero frequency shift and the intensity decreases monotonically with increasing frequency shift in a symmetrical manner about the origin. McTague and Birnbaum (Reference 18) introduced some minor improvements to this theory, including the idea that the scattering may be regarded as Raman scattering involving changes in the relative translational motion of atoms.

In order to explain the complete depolarization of their experimentally measured intensity in terms of the theory, it becomes necessary, unfortunately, to assume that the isotropic component of the induced polarizability is zero or nearly zero.

Refinements to this theory are provided by the work of Gersten (References 30 and 31), in which realistic interatomic potentials are employed, and the work of Lewis and van Kranendonk (Reference 32) in which interference effects are considered. Gersten found that the profile is given by a series of exponentials each one acting over a given range of frequency shift in succession. Except for frequency shifts less than 12 cm^{-1}, the scattered intensity increases with increasing temperature (!) and varies as the reciprocal of the reduced mass. The slope of the logarithm of the intensity versus frequency shift is predicted to vary as $T^{-1/2}$ and directly with the reduced mass at large frequency shifts.

Lewis and van Kranendonk discussed the interference effects which arise from the fact that the dipole moments induced in two successive collisions are not randomly oriented, but are most likely pointing in opposite directions. The interference is constructive leading to a maximum of scattered intensity at zero frequency shift

with a predominantly Lorentzian shape. The linewidth is proportional to the time between collisions which in turn is proportional to $T^{-1/2}$, the reciprocal of the density, and the square root of the atomic mass. It is expected that the interference effects in scattered light would not be observed at gas densities below 500 amagats.

In all of the theories based on scattering by collision pairs, it was necessary to assume that the isotropic component of the induced polarizability is zero, in order to fit the experimental data. Also, these theories evidently apply to gases at densities greater than about 100 amagats only. Under these conditions of high pressure, any van der Waals molecules that may be present very likely would be perturbed by a nearby atom and, hence, it would be more difficult to interpret scattering from such molecules. The experimental results presented here are in variance with important predictions of these theories and appear to be easier to interpret in terms of scattering by van der Waals dimers. Accordingly, the theory of Raman scattering by van der Waals dimers is briefly developed.

The formation of van der Waals molecules has been treated in detail by Stogryn and Hirschfelder (Reference 4). There are two types of bound states, physically

stable molecules with negative total energy and metastable molecules with positive total energy. The stable dimers must be formed in a three-body collision either as a simultaneous collision or as successive collisions with the formation of an intermediate state that is a metastable dimer. The third body is necessary, of course, to remove energy so that the dimer is left with a negative total energy. In a pure monoatomic gas, the stable dimers are formed, therefore, by the reactions

$$X + X + X \rightarrow X_2 + X^*$$

and

$$X + X \rightarrow X_2^*$$

$$X_2^* + X \rightarrow X_2 + X^*$$

where the asterisk indicates a more energetic species. It is also clear that the destruction of stable dimers must occur through collisions. Metastable dimers are formed by trapping of an atom behind the centrifugal hump in the effective interatomic potential. Whenever the intermolecular potential falls off faster than the reciprocal of the square of the interatomic distance, as it does

for van der Waals forces, such humps can occur in the effective potential. If the well corresponding to the hump is deep enough, a bound state can be formed. The dimer, thus formed, can decay by tunneling of one component through the hump. The lifetime of the metastable dimer is proportional to the effective width of the hump and does not depend on collision with another atom necessarily. At low gas densities the number of dimers of both types is proportional to the square of the density at constant temperature and (as shown by Stogryn and Hirschfelder) to $T^{-3/2}$ in first order at constant density.

The intensity I of light scattered by the van der Waals dimers is determined by the rules of quantum mechanics just as it is for ordinary molecules. The Raman intensity for a pure rotation band is given by (see, for example, Reference 37)

$$I = 64\pi^4\nu^4 c N_d S_J/Q \exp(-BhcJ(J+1)/kT)$$

where ν is the frequency of the scattered light, c is the velocity of light, N_d is the density of dimers, h is Planck's constant, B is the rotational constant of the dimer, k is Boltzmann's constant, T is absolute temperature,

J is the rotational quantum number, Q is the rotational state sum, and

$$S_J = \frac{3(J + 1)(J + 2)}{2(J + 3)}, \quad \Delta J = +2$$

$$S_J = \frac{3(J - 1)J}{2(2J - 1)}, \quad \Delta J = -2$$

The frequency shift $\Delta\nu$ for a pure rotation band is given by

$$|\Delta\nu| = 4B(J + 3/2)$$

In this work the rotational constants were found to be

$$B \doteq 0.04 \text{ cm}^{-1} \text{ for argon}$$

and

$$B \doteq 0.009 \text{ cm}^{-1} \text{ for xenon.}$$

Consequently, since Q is given by

$$Q = \sum_{J=0}^{\infty} (2J + 1) \exp(- BhcJ(J + 1)/kT),$$

it is quite reasonable to replace the sum by an integral over J to obtain

$$Q = \int_0^\infty (2J + 1) \exp(- BhcJ(J + 1)/kT)\, dJ$$

to good approximation (see Reference 11).

For the low resolution spectra the intensity I is measured over a wide band of frequencies which includes many rotational lines, as many as 70 for argon dimers and 300 for xenon dimers. Consequently, the formula must be summed over this frequency band to give the observed spectrum. (That is, the observed spectrum is the convolution of the true spectrum with the instrument profile.) For simplicity, it is assumed that the instrument profile is a constant over the frequency band and zero everywhere else. Replacing the sum by an integral, one has

$$I = I_o N_d \int_{J_1}^{J_2} S_J \exp(- BhcJ(J + 1)/kT)\, dJ$$

$$\cdot \int_0^\infty (2J + 1) \exp(- BhcJ(J + 1)/kT)\, dJ$$

where

$$I_0 = 64\pi^4\nu^4 c$$

J_1 is the rotational quantum number corresponding to the lower limit of the frequency band, and J_2 is that for the upper limit. Making use of the fact that $J \gg 1$, one notes that

$$S_J = 3/4J$$

and thus

$$I = 3I_oN_d/4\int_{J_1}^{J_2} J \exp(-\ BhcJ^2/kT)\ dJ$$

$$+ \int_0^{\infty} J \exp(-\ BhcJ^2/kT)\ dJ$$

$$= 3I_oN_d/4\ [\exp(-\ BhcJ_1^2/kT) - \exp(-\ BhcJ_2^2/kT)]$$

For a wide bandpass, $J_2 \gg J_1$, so that

$$I = 3I_oN_d/4\ \exp(-\ BhcJ_1^2/kT)$$

The frequency shift $\Delta\nu$ for large J is given by

$$|\Delta\nu| \doteq 4\ BJ$$

and therefore

$$J_1 \doteq |\Delta\nu|/4B$$

$$J_2 \doteq |\Delta\nu|/4B$$

Introducing the center frequency $\Delta\nu_0$ of the bandpass and the bandwidth w, given by

$$\Delta\nu_0 = (\Delta\nu_2 + \Delta\nu_1)/2$$

$$w = (\Delta\nu_2 - \Delta\nu_1)/2$$

one gets for the intensity

$$I = 3I_o N_d/4 \exp(-\ hc(|\Delta\nu_0| - w)^2/16\ kTB)$$

For $T > 222°K$ and the measurements on argon at least, the formulas given by Stogryn and Hirschfelder for N_d are valid and also the exponential may be expanded with retention of leading terms only, so that

$$I = 48\pi^4\nu^4 cN_d(1 - hc(|\Delta\nu_0| - w)^2/16\ kTB)$$

Stogryn and Hirschfelder (Reference 4) have calculated the densities of both physically stable (bound) and metastable dimers. The number of metastable dimers per cubic centimeter N_m and the number of physically stable dimers N_s are given by

$$N_m = \frac{2}{3}(.42991)\pi\sigma^3N^2(\epsilon/kT)^{3/2}\ [1 - 0.18963\ (\epsilon/kT)$$

$$+ .032311\ (\epsilon/kT)^2 - .0046995\ (\epsilon/kT)^3 + \ldots]$$

and

$$N_s = \frac{2}{3}(1.203604)\pi\sigma^3N^2(\epsilon/kT)^{3/2}\ [1 + .2539083\ (\epsilon/kT)$$

$$+ .05668206\ (\epsilon/kT)^2 + .01069780\ (\epsilon/kT)^3 + \ldots]$$

where σ and ϵ are parameters in the Lennard-Jones interaction potential. For argon at 120°K, $\epsilon/kT \doteq 1.0$ and for xenon at 222°K, $\epsilon/kT \doteq 1.0$ enabling one to retain only the leading terms of the series to good approximation. Since in the case of a perfect gas, $PV = NkT$ the number density of dimers at constant pressure P and volume V is given by

$$N_m = \frac{2}{3}(.42991)\pi\sigma^3\epsilon^{3/2}p^2V^2/(KT)^{7/2}$$

and

$$N_s = \frac{2}{3}(1.203604)\pi\sigma^3\epsilon^{3/2}p^2V^2/(kT)^{7/2}$$

To first order, therefore, for constant $\Delta\nu_0$

$$I \propto N_d$$

or

$$I \propto N^2\ T^{-3/2}$$

or

$$I \propto P^2\ T^{-7/2}$$

where N is the gas density. For xenon it appears that trimers are contributing to the scattering at T = 222°K and the theory of Stogryn and Hirschfelder, consequently, does not necessarily apply.

At constant temperature and pressure, the logarithm of the intensity is

$$\text{Ln } I = \text{Ln (constant)} - 7/2\ \text{LnT}$$

$$- hc(|\Delta\nu_0| - w)^2/16\ kTB$$

The slope of the intensity plotted versus wavenumber is

$$\frac{d\ \mathrm{Ln}\ I}{d|\Delta\nu_0|} = -\ hc(|\Delta\nu_0| - w)/8kTB \doteq -\ hc|\Delta\nu_0|/8kTB$$

In contrast to the result of the collision pair mechanism, the linewidth varies as T^{-1} and B^{-1}, instead of $T^{-1/2}$ and directly as the reduced mass of the pair of atoms.

C H A P T E R I V

EXPERIMENTAL APPARATUS AND TECHNIQUES

A block diagram of the complete apparatus is shown in Figure 1. All Raman spectra in this work were observed through the use of a 530 mm focal length Littrow-mounted triple monochromator (Reference 38) having a measured resolution of 0.35 cm^{-1} at 5145 Å and 0.4 cm^{-1} at 4880 Å, a reproducibility of 0.1 cm^{-1} in frequency, and very low stray light. The three monochromators were so arranged that the dispersions of the first two were additive and that of the last subtractive. Each monochromator had a dispersion of 10.5 Å/mm.

Intensity measurements were made using photon counting circuits and a chart recorder. The detector was an ITT FW 130 photomultiplier with an S-20 photocathode. The photomultiplier was cooled with a commercial thermoelectric cooler and generally had a dark count of 2 to 15 counts/second depending on cathode temperature. Full scale sensitivities used in recording Raman spectra were 50 counts/second, 100 counts/second, and 500 counts/second. For intensity measurements of the Rayleigh line, a neutral

Figure 1

Diagram of experimental apparatus

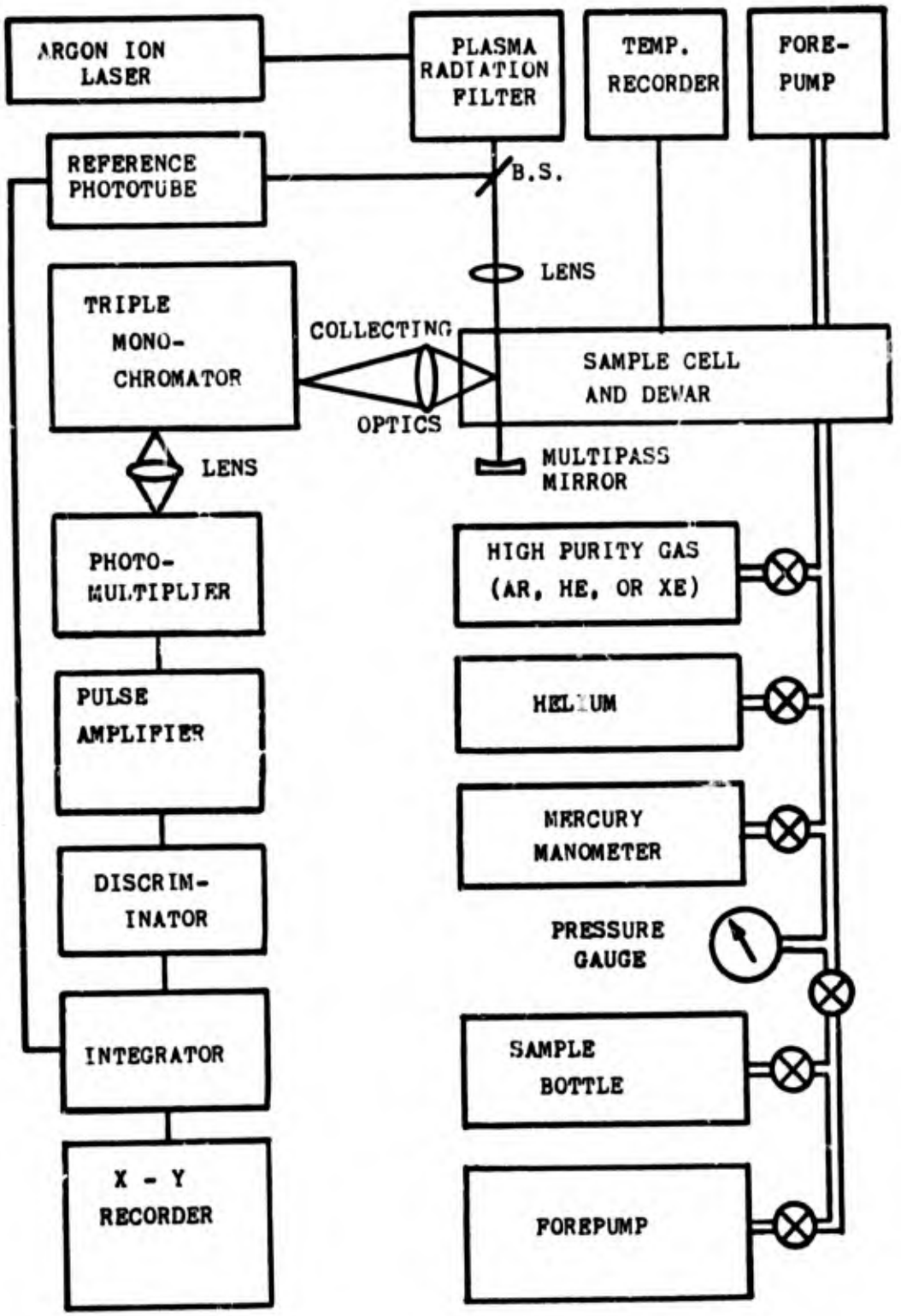
ARGON ION LASER
PLASMA RADIATION FILTER
TEMP. RECORDER
FORE-PUMP
REFERENCE PHOTOTUBE
B.S.
LENS
TRIPLE MONO-CHROMATOR
COLLECTING OPTICS
SAMPLE CELL AND DEWAR
LENS
MULTIPASS MIRROR
PHOTO-MULTIPLIER
HIGH PURITY GAS (AR, HE, OR XE)
PULSE AMPLIFIER
HELIUM
MERCURY MANOMETER
DISCRIM-INATOR
PRESSURE GAUGE
INTEGRATOR
SAMPLE BOTTLE
X - Y RECORDER
FOREPUMP

density filter of optical density equal to 4.0 was inserted in the beam and full scale sensitivities up to 20,000 counts per second were used.

Calibration of the system for intensity was made using a standard photometric lamp. The lamp was a commercial G.E. type 30A/T24/7 ribbon-filament lamp with a calibration traceable to the National Bureau of Standards (Reference 39). The direct substitution method was used for calibration of the Raman spectrometer for pen position versus intensity of the standard at selected wavelengths in the ranges of 20,486.3 cm^{-1} ± 50 cm^{-1} and 18,429.9 ± 50 cm^{-1} in which all Raman spectra were observed in this research. Figure 2 is a plot of measured intensity at constant wavelength versus the transmission of neutral density filters inserted at the aperture stop of the auxillary lens described below and in the beam from the standard lamp. The linearity of the response of the system can be seen to be quite good for the scale ranges used in the Raman spectra. The standard lamp, incidentally, was always operated at 25 amperes filament current and all readings were taken only after a warmup period of about one hour.

The wavelength sensitivity of the photocathode was determined by scanning the light from the standard

Figure 2

Calibration of spectrometer for light intensity at constant frequency shift (16 cm^{-1}).

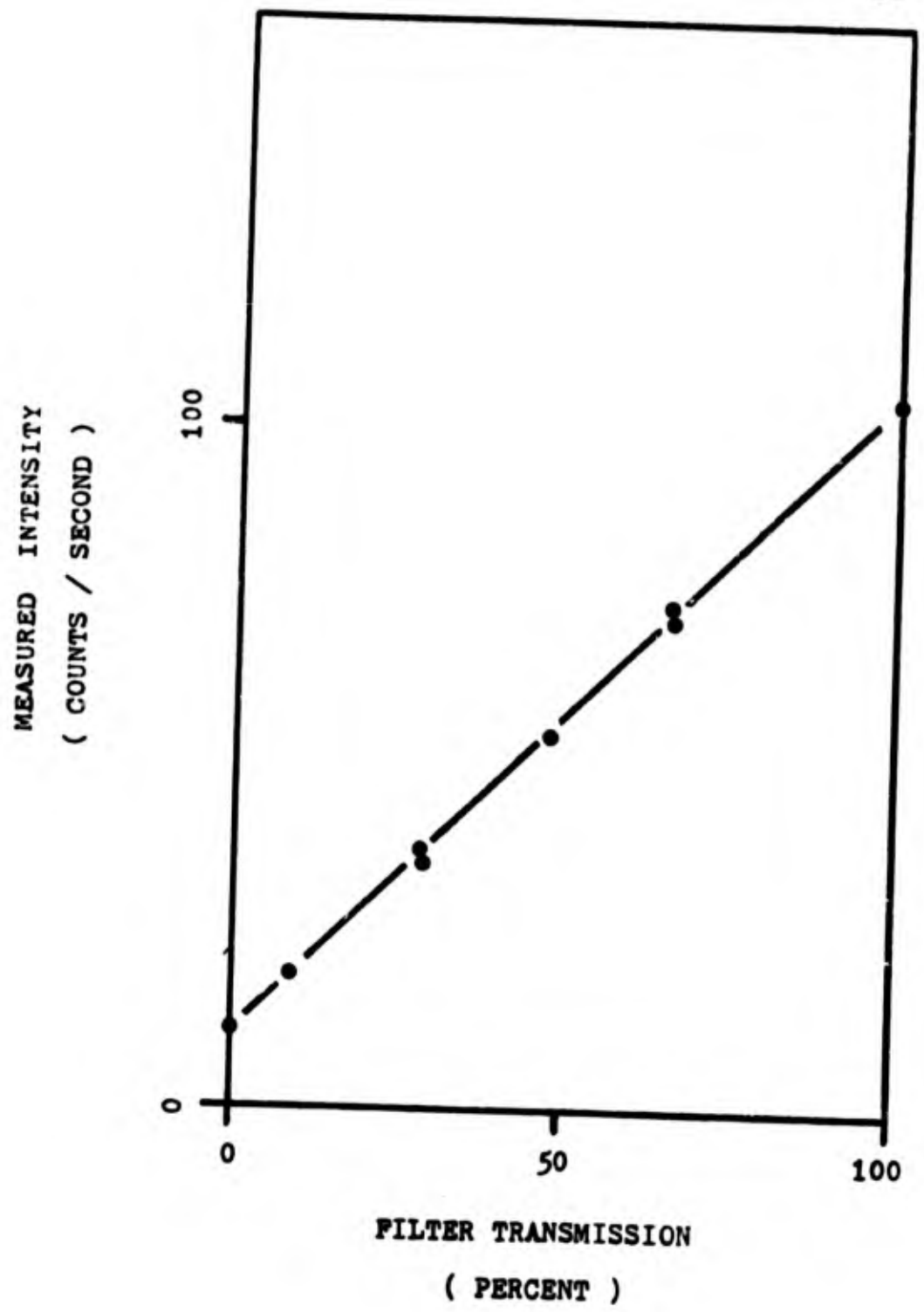
MEASURED INTENSITY
(COUNTS / SECOND)
100
0
0
50
100
FILTER TRANSMISSION
(PERCENT)

lamp for ± 50 cm^{-1} each side of the 4880 Å and the 5145 Å lines of the laser. The change in intensity from one extreme of the range to the other was no more than 2% of the total intensity. This change was in the direction expected from the blackbody curve of the standard lamp. In the range around the 4880 Å line where most of the spectra were taken the change in measured intensity over the range is essentially zero. The blackbody curve calculated by means of Planck's blackbody radiation law changes by not more than 2.5% over this range. It is evident, therefore, that the photocathode sensitivity decreases by less than 2.5% as the frequency decreases over the 100 cm^{-1} range centered about the 4880 Å line. Consequently, the variation of photocathode sensitivity with frequency may be safely ignored.

Because there was always some drift in alignment of the collecting optics and the monochromator optics of the system and because of drift in recording electronics (particularly in the reference signal system) it was necessary not only to align carefully the entire system before each experimental run, but also to check the recorded intensity against the standard lamp before each run. A relative intensity measurement was made in this case by

imaging the standard lamp filament through the sample cell and collection optics onto the entrance slit of the spectrometer. In this arrangement, an auxillary achromatic lens of focal length 191 mm and 45 mm diameter was used at 2 to 1 conjugates (demagnifying the filament by about two at the sampling point). Consequently, although the slit was completely and uniformly illuminated, the F/1 aperture of the spectrometer collection optics was not nearly filled. In spite of this defect, any changes of relative intensity, due to misalignment, drift of the electronics, laser power changes, or possible changes of the photocathode temperature, could be detected and the data corrected accordingly. The photometric lamp was kinematically interchangeable with a small MgO-coated integrating sphere, which was illuminated by deflecting the laser beam with a kinematic mirror system. The integrating sphere permitted alignment of the monochromators for maximum transmission before a run.

Except for those instances of strong Tyndall scatter or density changes, the scatter in the measured intensity data is given usually by $\pm\ 1/t\ (nt)^{1/2}$ to no more than $\pm\ 3/t\ (nt)^{1/2}$ where n is the measured intensity in counts per second and t is the integration time of

the photon counter. Integration times of either 50 or 100 seconds were used in all the runs.

The frequency calibration of the spectrometer was checked using the 20,486.3 cm^{-1}, 19,429.9 cm^{-1}, 20450.5 cm^{-1}, and 19,448.4 cm^{-1} lines of the laser (Reference 40) and by scanning the pure rotation spectra of air with the slits set at .35 cm^{-1}. The pure rotation spectrum of O_2 has been measured to ± 0.05 cm^{-1} by Weber and McGinnis (Reference 41). All Raman frequency shift measurements were made on the recorder chart paper by direct measurement of the displacement relative to the Rayleigh line peak. A precision of .02 cm^{-1} could be attained with this method, thus the accuracy of the frequency measurement was limited by the wavelength accuracy of the spectrometer.

Polarization measurements were made by a technique described by Claassen et al. (Reference 42) and Brandmuller et al. (Reference 43). The depolarization ratio for the 459 cm^{-1} line of CCl_4 was 0.008 as measured on the spectrometer by this method.

The sample cell was mounted in a vacuum dewar and fitted with fused-silica windows 2 mm thick. This arrangement permitted its use at gas pressures of from

1.5×10^{-3} torr to 3290 torr and temperatures from 77°K to 400°K. The laser beam passed through the cell by means of two windows at the Brewster angle and the scattered light from the gas passed to the spectrometer through a plane window at the front of the cell. A window at the rear of the cell permitted optical alignment of the laser beam to the spectrometer slit and passage of the light beam from the standard lamp into the spectrometer. The laser beam was passed about ten times through the sample volume by two small mirrors, one above the cell and on the axis of the incident beam and the other below the cell and to the side of the beam and each with its center of curvature at the sample volume. In this way the light intensity incident on the sample was increased. The sample cell could be filled or evacuated through a tube on its side sealed by a teflon plug. Through this tube a small thermocouple was inserted for measurement of the gas temperature. A small resistance heater was attached to the outside of the sample cell for adjusting the gas temperature to values above that of the liquid in the Dewar bath. An auxillary iron-constantan thermocouple was used to monitor the temperature of the sample cell. The small thermocouple used for gas temperature measurements inside

the cell was made from .001 inch diameter iron and constantan wires. The actual diameter of the thermoelectric junction was usually around .003 inch. The output of the thermocouple was recorded continuously during runs by a strip chart recorder. The thermocouples were calibrated with boiling water, liquid nitrogen, frozen methanol and ethanol, ice water, and dry ice. The readings so obtained were always not more than 2°K less than the correct temperature as given by a standard table of e.m.f. verus temperature (Reference 44). The calibration points of the thermocouple compared to the standard e.m.f. values are shown in Figure 3.

Pressures were measured with a Bourdon tube absolute pressure gauge with a scale range 0-100 psia and accuracy of 1% of full scale and also with a mercury manometer having a range of 0-2400 Torr plus one atmosphere and an accuracy of ± 5 Torr. The calibration of the pressure gauge against the mercury manometer is shown in Figure 4 from which it can be seen that the linearity and reproducibility is very good.

The exciting line was generated by an argon-ion laser which has a measured power of 3.5 watts in the 5145 Å line and 2.7 watts in the 4880 Å line. All observations

Figure 3

Typical calibration curve of iron constantan thermocouple used in sample cell.

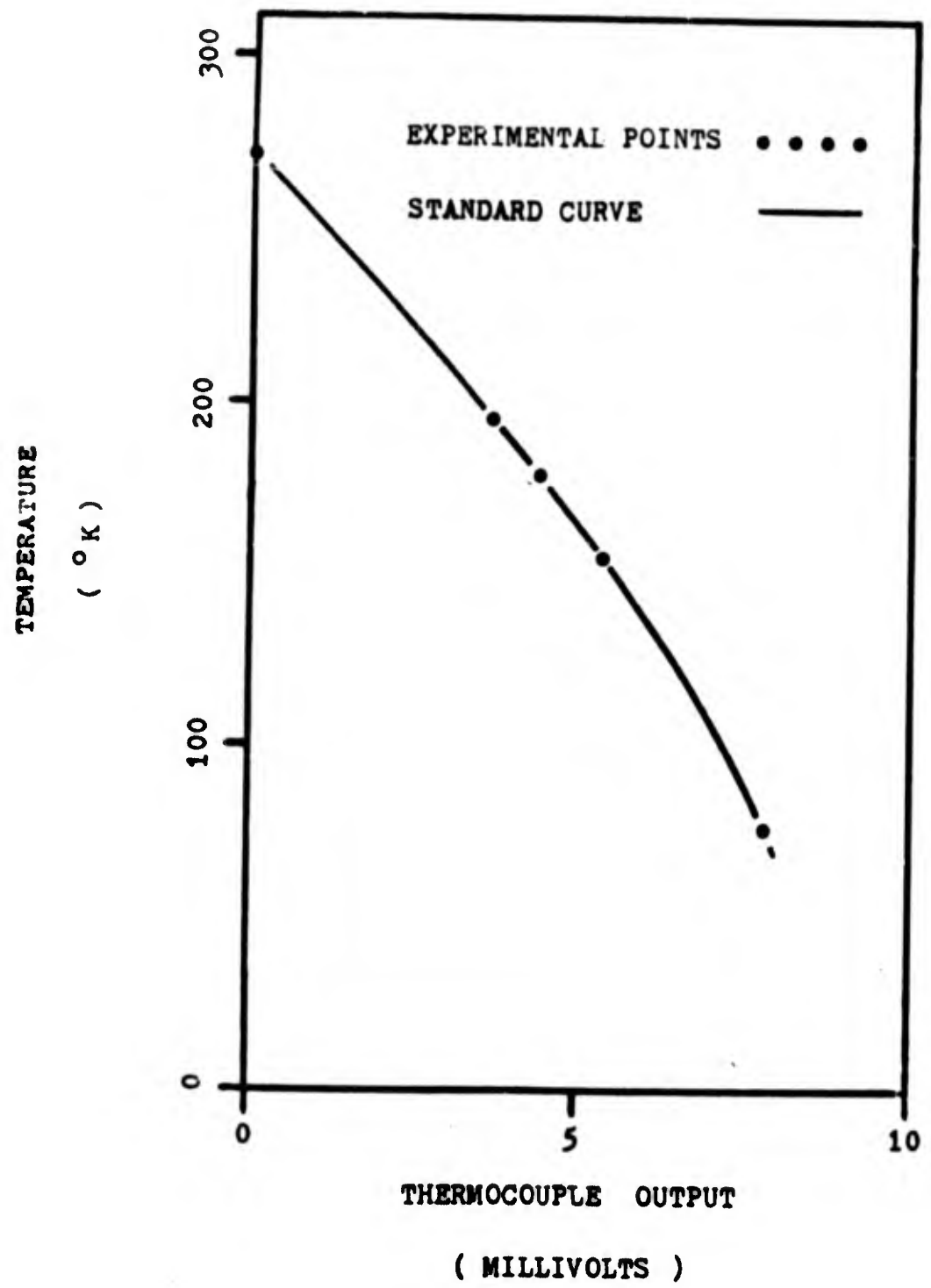
EXPERIMENTAL POINTS
STANDARD CURVE
TEMPERATURE
(°K)
300
200
100
0
0
5
10
THERMOCOUPLE OUTPUT
(MILLIVOLTS)

Figure 4

Calibration of gauge pressure against the mercury manometer.

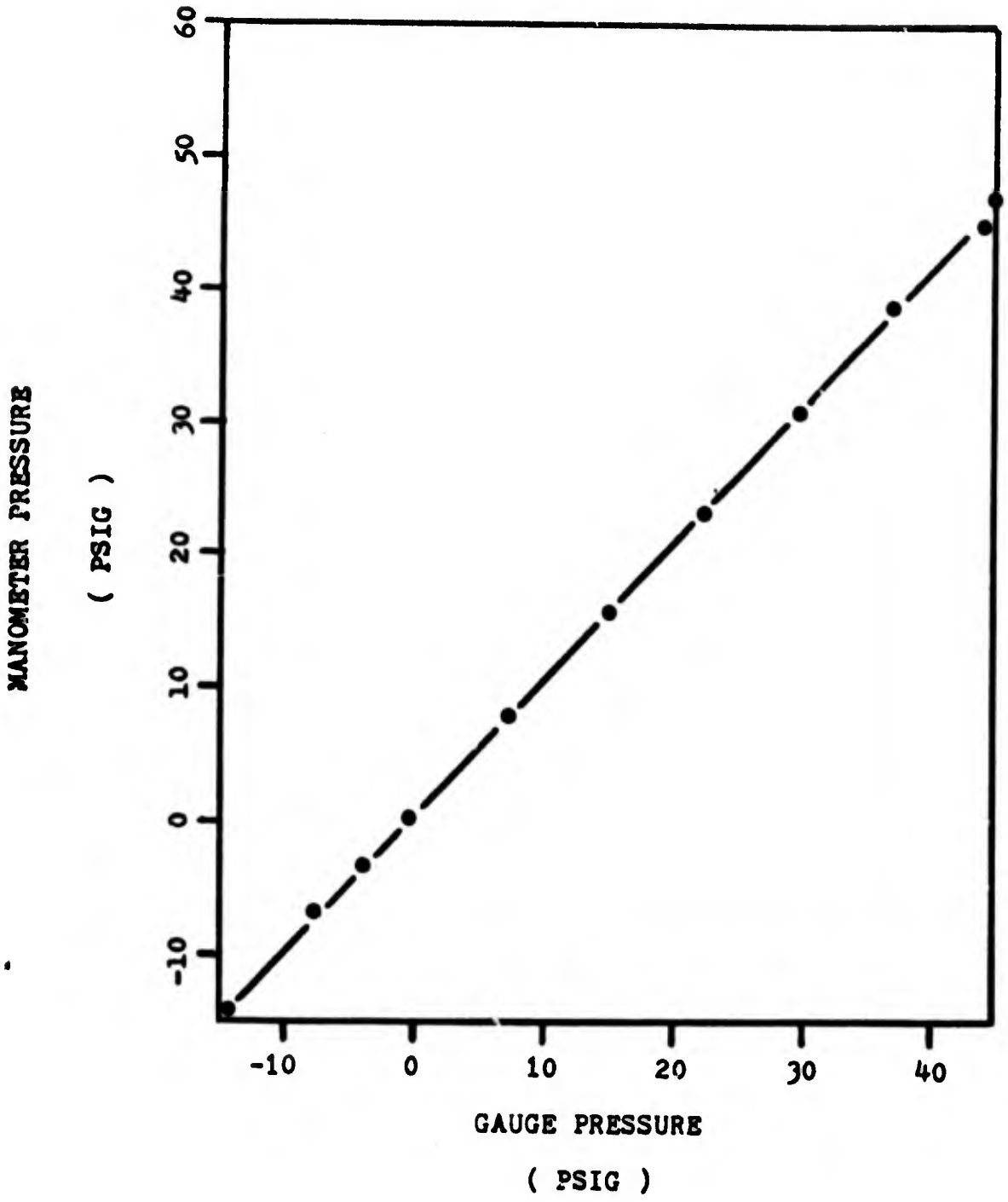
MANOMETER PRESSURE
(PSIG)
60
50
40
30
20
10
0
-10
-10
0
10
20
30
40
GAUGE PRESSURE
(PSIG)

of spectra were made with the laser at full power or within 25% of full power. A right angle scattering geometry was used in which the laser beam was directed vertically upward into the sample cell and in which the optic axis of the collection optics of the Raman spectrometer was in a horizontal plane and perpendicular to the laser beam. The electric vector of the laser light was in the horizontal plane and perpendicular to the optic axis of the spectrometer collection optics. In all measurements of spectra the relative aperture of the collection optics was F/1. Before reaching the sample cell, the laser beam passed through a prism and slit system similar to that developed by Claassen et al. (Reference 42) and designed to remove the plasma radiation of the laser. Actual measurement of the effectiveness of plasma line filtering was made by detuning the laser at full plasma current so that no lasing occurred and scanning the entire frequency range over which spectra were obtained. Detuning the laser reduced the intensity of the laser lines to zero but left the intensity of the plasma radiation practically unchanged. No signal other than dark count was observed at anytime during this scan.

In all runs, before spectra were taken, it was necessary to allow Tyndall scattering from dust particles

or, at the low temperatures, from liquid droplets to subside. Tyndall scattering was particularly acute after a pressure change at low temperatures. The laser beam in the sampling volume was, therefore, inspected visually at intervals. When the Tyndall scattering reached a value corresponding to less than one scintillation per minute in the sample volume, the run could be started with good assurance that the noise from Tyndall scattering would be essentially undetected. It generally took about one hour to as long as two or three hours before a run could be started. By this time, however, temperatures and pressures were well stabilized.

The gases used in this work were Linde ultrahigh purity "gold label" argon, Linde research grade helium, Linde research grade hydrogen, and Linde research grade xenon. Table I lists the analysis of each gas as reported by the manufacturer.

In addition, after a number of experimental runs, samples were taken of the gas in the cell and mass spectra recorded. In some cases, the gas had been in the sample cell for as long as a week during most of which time it was subjected to the full intensity of the laser beam. This procedure ensured that any gaseous impurities, which

TABLE I

MANUFACTURERS' SPECIFICATION OF

PURITY OF GASES

ARGON	
Ar	99.999%
N_2	3 ppm
O_2	1 ppm
Total Hydrocarbons	1 ppm
H_2O	1 ppm
XENON	
Xe	99.995%
Kr	20 ppm
N_2	5 ppm
O_2	1 ppm
H_2	1 ppm
Total Hydrocarbons	1 ppm
H_2O	1 ppm
HELIUM	
He	99.9995%
Ne	2 ppm
N_2	1 ppm
O_2	1 ppm
H_2	1 ppm
Total Hydrocarbons	1 ppm
H_2O	1 ppm

might be formed through the action of the laser beam on dust particles (some were always blown into the cell during filling) or other material that might inadvertently come into the laser beam, would be detected. In all cases only minor amounts of a few impurities were found. These were nitrogen, butane, and possibly water vapor. Water and butane should have even lower, and thus completely undetectable, concentrations at the lowest temperatures of some of the experimental runs. Also no pure rotation band of nitrogen was observed in any of the experimental runs presented here. In helium no impurities were observed with the mass spectrometer. There were some argon samples which contained about four parts of H_2O in a hundred thousand and about five parts of N_2 in a hundred thousand. In a few of the argon samples about four parts of butane in a hundred thousand were detected. The butane was always detected in samples taken in sample bottle number four and the concentration of butane decreased to zero after the first few times bottle number four was used. In xenon about one part of H_2O in a hundred thousand and the same concentration of N_2 were detected in most of the samples. One sample of xenon contained about five parts per thousand of air and one part per hundred

thousand of a lightweight hydrocarbon. This sample had been accidentally contaminated with air when the sample bottle was filled. Most of the impurities observed could very likely be in the mass spectrometer background since all except O_2 and butane were present in the background scans of the mass spectrometer.

The maximum sensitivity of the Raman spectrometer is such that perhaps a concentration as low as one part per ten thousand of a very strong scatterer could be detected. It seems reasonable to conclude that it is extremely unlikely that the observed spectra are due to impurities in the gases.

In an investigation of this type, stray light is always a potential source of false spectra. Three possible sources of stray light occur in the apparatus used in this experiment; namely, scattering from the sample cell, nonuniform illumination of the entrance pupil by the collection optics, and stray light in the monochromator. Stray light from the laboratory room was eliminated by the simple expedient of locating the apparatus in a photographic dark room and turning out the lights during runs. Some time was spent in investigating stray light from the various types of sample cell and it was

found that the windows of a cell produce a great deal of light shifted in frequency compared with the walls of the cell. The cell windows fluorese and produce a Raman spectrum of their own where the full intensity of the laser beam strikes them. This light finds its way into the field of view of the collection optics by a light pipe effect and by direct transmission, if the walls of the cell are transparent, and by multiple reflections from the cell walls and windows themselves. The best way to eliminate the direct transmission and light pipe effect was to use a metal cell and locate the windows a suitable distance determined by the geometry of the system from the sample volume. Glare baffles external to the cell further attenuated this light. Multiple reflections were reduced by oxidizing the cell, which was made from Invar, until it was a flat black color and by appropriate geometrical configuration of the cell. It was particularly important to ensure that the parts of the cell in the immediate cone of view of the collection optics were so shaped as to reflect most of the light away from the collection optics. In addition, walk-off of the laser beam between cell windows and reflections from the windows was minimized by placing the windows on the cell at the Brewster

angle and parallel to 15 minutes. The entire dewar could be tilted so that the windows were very close to the Brewster angle for the laser beam. Striae-free, nonfluoresing fused silica windows with 0-0 surface finish were used in the laser beam. It was also desirable to keep all the windows very clean. Background scatter of the sample cell could not be completely eliminated by these procedures, but it was greatly reduced and had a completely flat variation with frequency except at the Rayleigh line. The measured background from the vacuum cell usually did not exceed 35 counts per second at any of the temperatures of the experiment and this intensity included 12 counts per second photomultiplier dark current plus about 2 counts per second from the sample cell thermocouple.

The uniformity of illumination of the aperture of the collection optics usually was a matter of alignment of the sample cell to the image of the monochromator entrance slit formed by the collection optics. This uniformity was investigated during scans over the frequency ranges of the experiment by visually observing a MgO coated screen inserted at the exit pupil of the collection optics. When the alignment was good no nonuniformity appeared during the scan. The precision of alignment depended on

the F number of the collection optics and the drift of relative position of the optic axis of the collection system with respect to the sample cell. This process, however, was of completely negligible consequence under the conditions of the experiment. A more serious effect was that due to the drift of the position of the laser beam relative to the image of the entrance slit. Investigation showed that this effect depended mainly on temperature of the sample cell and dewar and on the slitwidth. For slitwidths greater than 1 cm^{-1}, the drift produced no measurable effect for periods of 16 to 24 hours provided the temperature of the apparatus had sufficiently stabilized. This problem was alleviated by alignment of the apparatus before each series of scans.

The monochromator was specially designed by the manufacturer to reduce stray light due to multiple reflections between the mirrors and diffraction gratings. This type of stray light is the principal cause of spurious band structure in Ebert, Littrow, and Czerny-Turner mounted grating monochromators (Reference 38). It is eliminated completely by arranging the camera and collimating mirrors with reference to the grating so that the projection of the normals to the surfaces of the mirrors do not pass

through the grating for any rotation of the grating about its scanning axis. Another source of spurious band structure in the triple monochromator was misalignment of the three monochromators both relative to each other and relative to the optical components of an individual monochromator. This type of misalignment could be easily detected by scanning the Rayleigh line for the vacuum cell, since it is present independently of the contents of the sample cell. An experimental investigation was made by purposely misaligning the triple monochromator and observing the Rayleigh line. In general, the effect could only be observed about the Rayleigh line, because even small misalignments entirely wiped out peaks of lesser intensity. For a triple monochromator, at least, anywhere from one to three peaks could be obtained by scanning the Rayleigh line with a misaligned instrument. The intensity of the peaks varied in an unpredictable way with the degree of misalignment. However, the spacing (in cm^{-1}) between adjacent peaks varied from zero for perfect to near perfect alignment up to a maximum separation a little above the slitwidth (full width at half height in cm^{-1}). After that point, further misalignment simply wiped out the Rayleigh line. In no instance could adjacent

peaks be separated greater than twice the slitwidth (in cm^{-1}) without loss of transmission. The smaller the slitwidth, the smaller the degree of misalignment required to produce spurious peaks. On the other hand, the wider the slits were set, the greater the degree of misalignment required before a splitting of the Rayleigh line could be discerned, the initial effect being a reduction of transmission. It may be concluded that peaks in the spectra separated by greater than twice the slitwidth cannot be caused by monochromator misalignment.

In any case, spurious band structures due to stray light could be identified by scanning the vacuum cell or high pressure helium which gave practically no scattering itself (except, of course, Rayleigh scattering). Experimental runs, in which band structures were observed, were repeated with the vacuum cell or with both the vacuum cell and then helium. In no such run were spurious band structures detected.

Because of the requirement that a laser beam must pass through the dewar and the sample cell, the sample cell was in contact with the cooling bath only at one end. Heating of the cell windows at the other end by the laser beam and heat leakage through the gas filler tube created

thermal gradients in the gas in the cell. There was the additional possibility that the laser heated the gas directly by absorption of light from the beam. These effects were investigated by means of the small thermocouple inside the sample cell. Figure 5 shows the results of measuring the temperature at different distances from the laser beam. It should be noted that with the laser off the temperature of the thermocouple is the same as that of the laboratory room, namely 298°K and, when the laser is turned on, the thermocouple temperature instantly rises to 301°K. This behavior is good evidence that the thermocouple is mainly heated by absorption of radiation from the laser directly and not appreciably heated by the gas. In fact, it must be cooled by the gas! The emissivity and absorptivity of the thermocouple were not measured, but a value of 0.5 for both is likely. An upper limit for the absorptivity of argon, xenon, and helium may be estimated from the Rayleigh scattering data taken in this experiment by assuming that all the energy scattered really goes into translational motion of the gas molecules. The ratio of the intensity absorbed, I_a, to the intensity incident in the laser beam I_L is given by

Figure 5

Thermocouple temperature as a function of distance from the laser beam at full laser power.

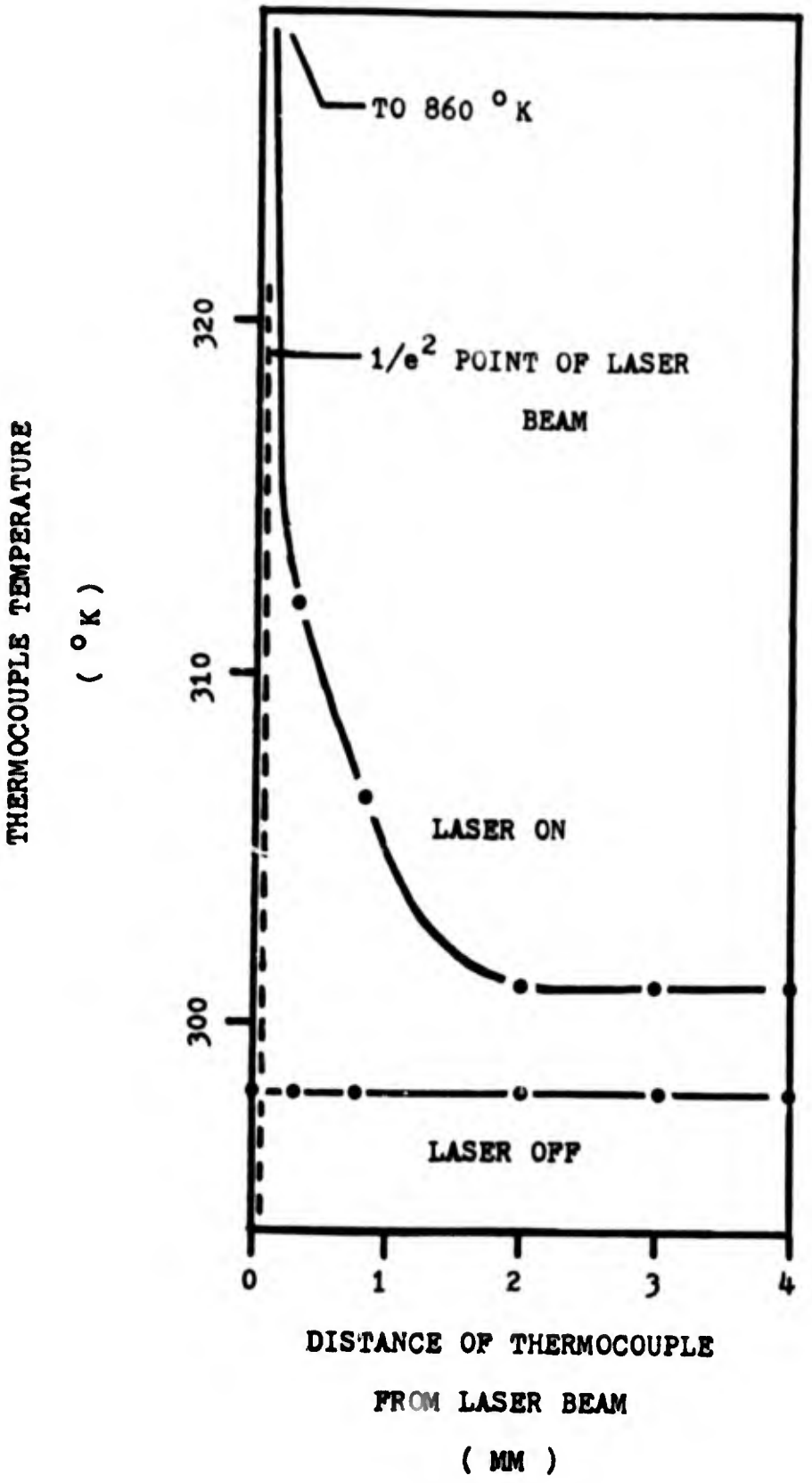
TO 860 °K
320
1/e² POINT OF LASER BEAM
310
LASER ON
300
LASER OFF
0
1
2
3
4
THERMOCOUPLE TEMPERATURE
(°K)
DISTANCE OF THERMOCOUPLE
FROM LASER BEAM
(MM)

$$\frac{I_a}{I_L} = \frac{P_a}{P_L} = \frac{4\pi nhc\nu x10^{-7}}{wT_m g P_L} = a$$

where a is the estimated absorptivity, P_a is the power absorbed by the gas, P_L is the power incident in the laser beam, n is the observed number of photons per second, w is the solid angle over which light is collected, h is Planck's constant, c is the velocity of light, ν is the frequency of the laser light in cm^{-1}, T_m is the transmission of the spectrometer and g the photomultiplier quantum efficiency. The transmission of the spectrometer is about 20%. The quantum efficiency of the photomultiplier is about 0.15, so that for the 4880 Å line,

$$a = \frac{16n(2 \times 10^{-6})(2 \times 10^{4})(10^{-7})}{(.2)(.15)(.27)} \doteq n \times 10^{-16}$$

for helium, $n \doteq 10^5$, for argon, $n \doteq 10^7$, and for xenon, $n \doteq 10^8$. Consequently,

$a \doteq 10^{-11}$ for helium,

$a \doteq 10^{-9}$ for argon,

$a \doteq 10^{-8}$ for xenon.

It can readily be seen that if radiation is the main source of heating, the direct heating of the gas by the laser should be quite negligible. The curve in Figure 5 therefore may be more of a measure of the intensity profile of the laser beam in the sample cell than a measure of the gas temperature.

Another possibility is that the curve is a temperature profile of a convection current flowing upward from the bottom cell window (through which the laser beam passes), at least for distances outside the $1/e^2$ points of the laser beam. However, the almost instantaneous decrease of thermocouple temperature when the laser beam is interrupted precludes this mechanism as the major cause of heating. In Figure 6 is given strong evidence that convection is not involved to a large extent at least in heating the thermocouple near the laser beam. Not only is the thermocouple temperature higher when the cell is evacuated, but the rate of increase of temperature with laser power is greater by a factor of 2 than that with the cell full of argon. This result does not rule out conduction of heat through the wires of the thermocouple or a small amount of convection directly from the gas in the laser beam. The former is unlikely because of the

Figure 6

Thermocouple temperature as a function of laser power;
5145 Å laser line, 1mm from beam.

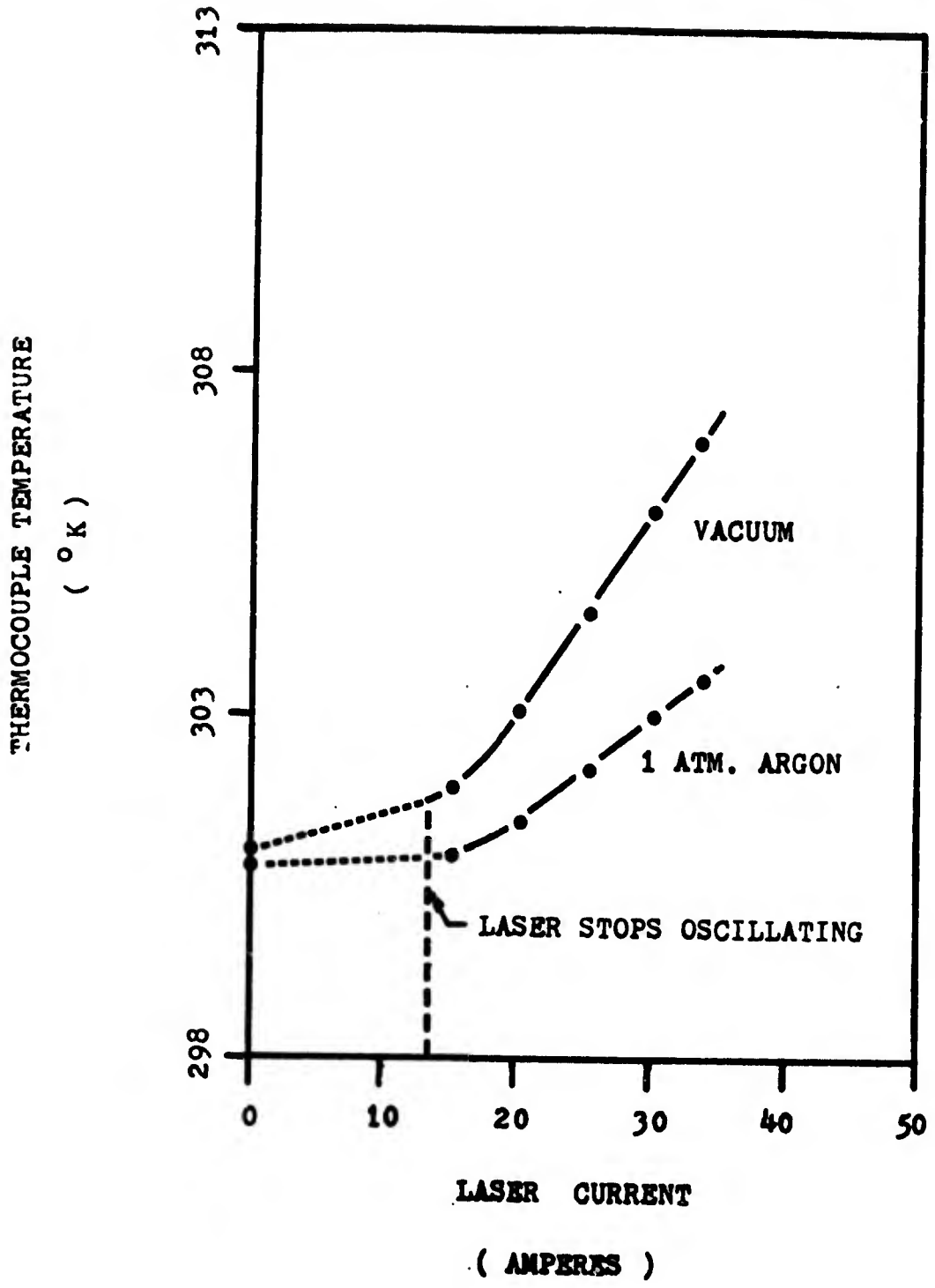
313
308
303
298
THERMOCOUPLE TEMPERATURE
(°K)
VACUUM
1 ATM. ARGON
LASER STOPS OSCILLATING
0
10
20
30
40
50
LASER CURRENT
(AMPERES)

small diameter of the thermocouple wire. In addition, the beam of the thermocouple could be placed in the cold gas streaming from a cake of dry ice and the wire changed to a temperature of 300°K 10 mm away without measurably affecting the temperature reading for dry ice.

All these considerations lead one to believe that the temperature curve in Figure 5 can be explained by two mechanisms: radiation heating of the thermocouple by laser light for $0 \leq r \leq r_0$ where r_0 is the $1/e^2$ point of the laser beam, and r is the distance from the center of the laser beam; and heating of the thermocouple by thermal convection of argon directly from the hot spot caused by the laser beam on the cell window. The temperature is then given by the sum of two Gaussian functions, one arising from the radiant heating by the laser beam and the other from thermal convection of argon from the hot spot on the lower cell window.

The convection problem is treated first by a simple model. Suppose the hot argon is formed at the hot spot on the window and moves vertically at uniform velocity to the region of the thermocouple. As the hot argon moves upward it spreads radially according to the laws of diffusion. The temperature distribution is given by

$$\nabla^2 T = (C\rho/\kappa) \frac{\partial T}{\partial t}$$

where C is the specific heat, ρ is the density, and κ is the thermal conducitivity of argon. The initial condition is $T(r,0) = T_0\delta(r)$, where the hot spot is at r = 0. Solving the differential equation, one gets

$$T = (T_1/2t) \exp(- C\rho r^2/4\kappa t)$$

The time t at which the temperature is measured is the time it takes for the argon to reach the plane of the thermocouple by convection. If the convection velocity is v and the distance from the window to the thermocouple plane is s, then t = s/v and

$$T = (T_1 v/st) \exp(- C\rho v r^2/4\kappa s)$$

The radiation heating case is determined by setting the power absorbed from the laser beam equal to the heat losses. At the high temperatures reached by the thermocouple in the laser beam, conduction losses through the wires and convection losses are important. Consequently,

$$a_T P_L = 10^{-7} e_T \sigma A_T (T - T_s)^4$$

$$+ 4.2(\kappa_w A_w / x_w + H_a A_T)(T - T_s)$$

where a_T is the absorbance of the thermocouple, P_L is the power of the laser beam, e_T is the emissivity of the thermocouple, σ is the Stefan-Boltzmann constant, A_T is the surface area of the thermocouple, T_s is the temperature of the surroundings, κ_w is the thermal conductivity of the wire, x_w is the length of the wire, A_w is the cross-sectional area of the wire, and H_a is the heat transfer coefficient for convection defined by Ingersoll (Reference 45). Let

$$a_1 = 4.2 \times 10^7 / e_T \sigma A_T (\kappa_w A_w / x_w + H_a A_T),$$

$$a_0 = - a_T P_L \times 10^7 / e_T \sigma A_T ,$$

and

$$u_1 = [a_1^2/2 + (- 64a_0^3/27 + a_1^4/4)^{1/2}]^{1/3}$$

$$+ [a_1^2/2 - (- 64a_0^3/27 + a_1^4/4)^{1/2}]^{1/3}$$

then

$$T - T_s = 1/2[u_1^{1/2} + (4(u_1^2/4 - a_0)^{1/2} - u_1)^{1/2}]$$

The intensity profile of the laser beam is Gaussian, so that for the laser power one has

$$P = 2P_0/\pi^{1/2} r_0 \exp(-2r^2/r_0^2)$$

where P_0 is the total power in the beam and r_0 is the $1/e^2$ point of the beam. In order to get a useful result from the these equations they must be approximated. Note that, if $-a_0$ is much greater than a_1, then

$$T - T_s = (-a_0)^{1/4}$$

and, if a_1 is much greater than a_0, then

$$T - T_s = (a_1)^{1/3}$$

The former case occurs when r is small and the latter when r is large. A very crude approximation can be made by taking the solution to be the sum

$$T - T_s = (- a_0)^{1/4} + f(r)(a_1)^{1/3}$$

where f(r) obeys the following conditions

$$\lim_{r \to 0} f(r) = 0$$

$$\lim_{r \to \infty} f(r) = 1$$

Note that already

$$\lim_{r \to \infty} (- a_0)^{1/4} = 0$$

Further, since u_1 depends on r only through a_0, it seems reasonable to take f(r) to be some function of a_0. The simplest one is

$$f(r) = 1 - (- a_0)^m$$

Consequently

$$T - T_s = (- a_0)^{1/4} + (1 - (- a_0)^m)(a_1)^{1/3}$$

Finally,

$$T - T_s \doteq \left(\frac{2\, a_T\, P_0}{\pi^{1/2} e_T \sigma A_T r_0} \right)^{1/4} \exp(-\, r^2/2r_0^2\,)$$

$$+ (4.2 \times 10^{-7}/e_T \sigma A_T(\kappa_w A_w/x_w + H_a A_T))^{1/3} \left[1 \right.$$

$$\left. - \left(\frac{2\, a_T P_0}{\pi^{1/2}\, e_T \sigma A_T r_0} \right)^m \exp\,(-\, 2m r^2/r_0^2) \right]$$

The above results suggest fitting the data to two Gaussian curves, one for the thermal convection and the other for the radiation heating. A good fit is obtained with the equation,

$$T = 548 \exp(-\, r^2/(.102)^2) + 11.0 \exp(-\, r^2/(.987)^2) + 301$$

which is shown as the continuous line in Figure 5. The first term is the radiation heating while the second term in this equation presumably describes convection. If the suppositions are correct, the true temperature T_g of the gas is given by the last two terms of the equation, thus,

$$T_g = 11.0 \exp(-\, r^2/(.987)^2) + 301$$

Extrapolation to r = 0 gives the gas temperature in the laser beam to be 312°K as compared to 301°K measured by the thermocouple in the position it usually had during experimental runs. It may be concluded that the actual temperature of the gas in the sample volume of the beam could be about 11°K higher than the measured value.

Since it was impossible to move the thermocouple more than a few millimeters, temperature gradients in the cell were investigated by varying the pressure of the gas (and, thus, the thermal conductivity). Typical results are plotted in Figure 7. The curves flatten out as 300°K is approached. The thermal gradients are caused primarily by heat leaking to the cell through the gas filling tube and, to a lesser extent, by heating of the sample cell windows with the laser beam. The thermal gradients became troublesome only very near the boiling point of the gas being studied, since at this point they are accompanied by relatively large density gradients in the gas which cause fluctuations of the intensity of the scattered light that in turn make it difficult to record spectra. This was true in spite of the fact that, when the density was increased, the average temperature gradient from the front to the back of the cell in the gas was decreased under

Figure 7

Thermocouple temperature as a function of gas pressure;
4880 Å laser line, 2.7 watts, 1mm from beam.

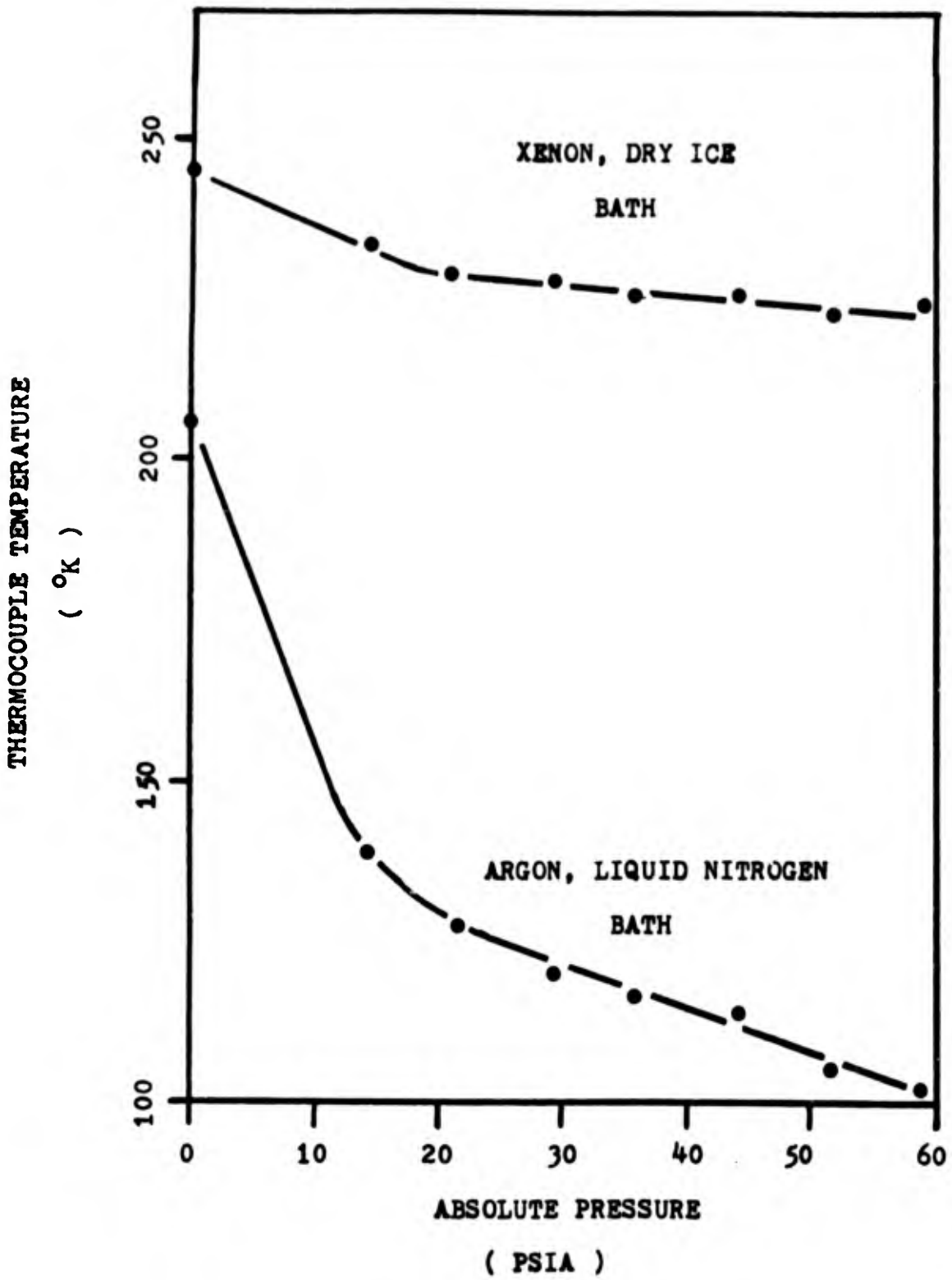
THERMOCOUPLE TEMPERATURE
(°K)
250
200
150
100
XENON, DRY ICE
BATH
ARGON, LIQUID NITROGEN
BATH
0
10
20
30
40
50
60
ABSOLUTE PRESSURE
(PSIA)

these conditions. Striae due to the density fluctuations could readily be observed in the gas, especially when there was boiling liquid in the cell. As a consequence of the density fluctuations, spectra recorded near 90°K in argon and 190°K in xenon were too noisy to be useful. In the case of argon, the maximum average temperature gradient from the thermocouple at the front to the back of the cell (with boiling argon at the back of the cell) was -0.4°K/mm and occurred at the lowest pressure, namely one atmosphere, at which spectra were recorded. In the case of xenon the maximum average gradient was -0.1°K/mm. Since the thermocouple was placed 2 mm from the laser beam during experimental runs, the error in temperature measurement from this source is considered negligible.

C H A P T E R V

EXPERIMENTAL RESULTS

An important problem in nearly all Raman spectroscopy is producing sufficient scattered light intensity to record a signal, and the research reported here is no exception to this rule. In fact, the greatest difficulty of this experiment was obtaining a signal to noise ratio greater than one. Nevertheless, it was still possible to record spectra for argon and xenon. The rapid decrease of light transmission of the monochromator (see Figure 8) with slitwidth precluded obtaining spectra when a resolution greater than that corresponding to 1.8 cm^{-1} slitwidth for argon and 0.8 cm^{-1} for xenon was used.

In the case of helium, no light scattering was observed except for a slight amount at the lowest temperature (126°K) and the highest pressure (3113 mm Hg) reached for helium and with the use of 6 cm^{-1} slitwidth. It was, therefore, not possible to investigate the dependence of this scattering on temperature and gas density, so that little significance can be attached to it.

On the other hand, the scattering from argon and xenon was considerably stronger and spectra were

Figure 8

Variation of measured intensity with monochromator slitwidth.

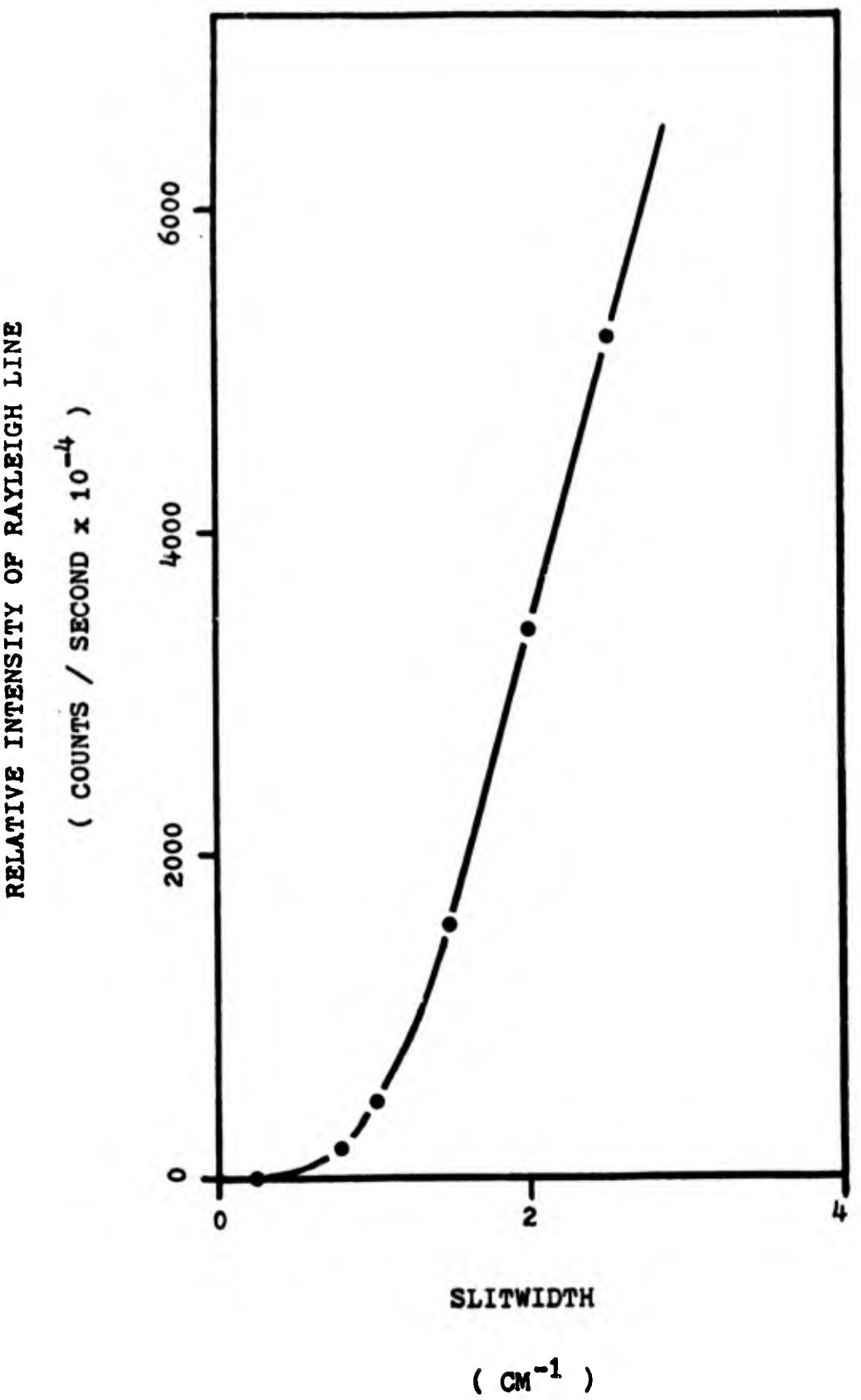
RELATIVE INTENSITY OF RAYLEIGH LINE
(COUNTS / SECOND x 10^{-4})
0
2000
4000
6000
0
2
4
SLITWIDTH
(CM^{-1})

obtained for these gases. All of the spectra reported here were taken with the 4880 Å line of the laser, because the presence of a laser line at 16.5 cm^{-1} on the anti-Stokes side of the 5145 Å line made it difficult to determine the symmetry (or lack of it) of the spectra with respect to the Rayleigh line. The density dependence of the scattered intensity, temperature variation of scattered intensity, and the Raman spectra were determined for argon also with the 5145 Å laser line and no essential difference from the results obtained at 4880 Å could be detected.

At high resolution (1.8 cm^{-1} slitwidth) a continuous band structure was observed in the Raman scattering from argon. High resolution spectra for argon at temperatures of 300°K, 152°K, and 103°K and a pressure of 3140 mm Hg are shown in Figure 9. It can be seen that the band structure strongly resembles an unresolved pure rotation band of a diatomic molecule. The peaks of the band occur at a frequency shift of ± 8.3 ± .5 cm^{-1} from the Rayleigh line peak and move to about ± 5.5 ± .5 cm^{-1}, becoming shoulders on the Rayleigh line when the temperature is decreased to 152°K. With further decrease of temperature to 103°K the peaks disappear altogether, presumably having moved even closer to the Rayleigh line.

Figure 9

High resolution Raman spectra of argon at 3140 mm Hg pressure, 1.8 cm^{-1} slitwidth, 4880 Å laser line.

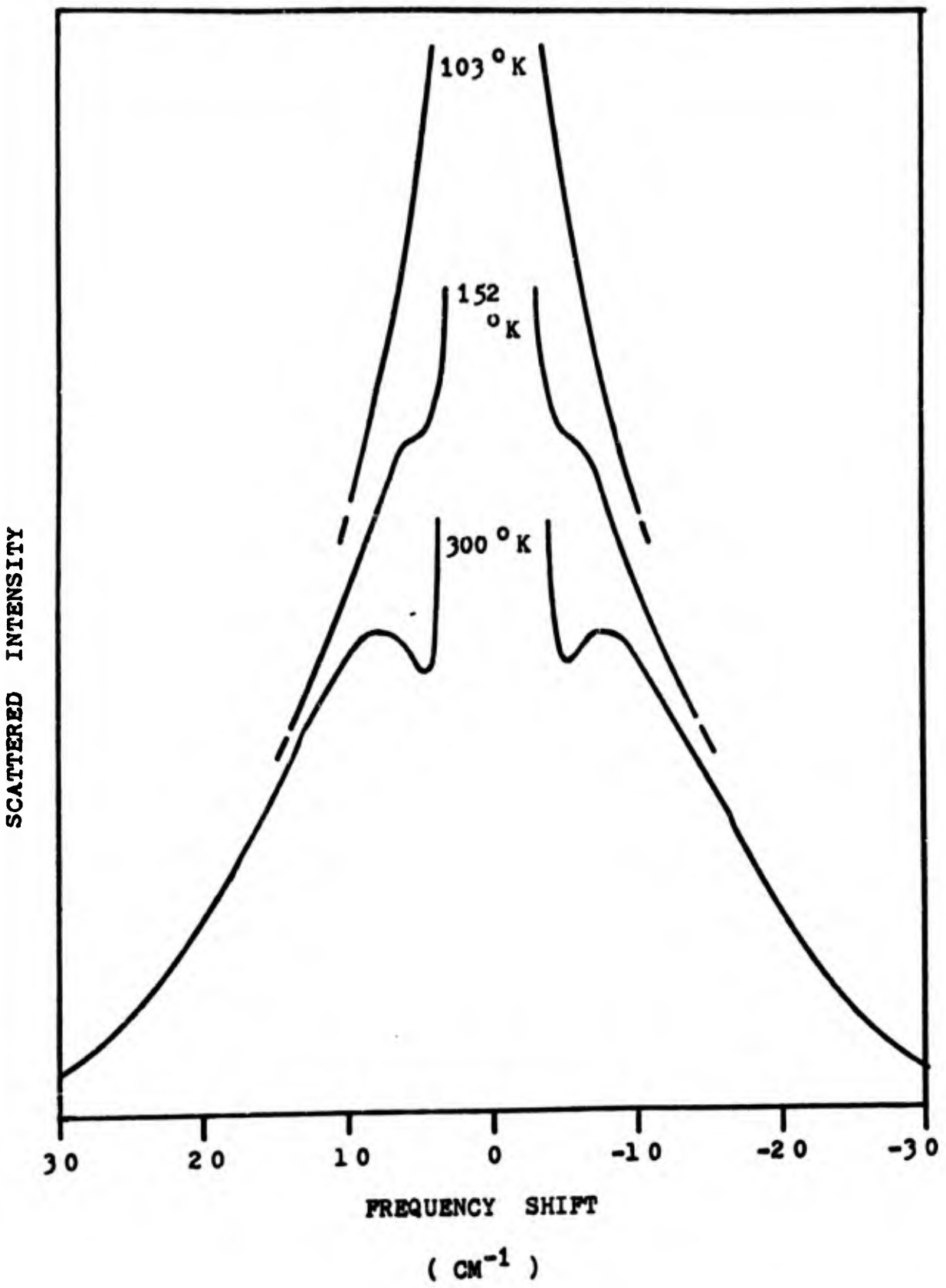
103 °K
152 °K
300 °K
SCATTERED INTENSITY
30
20
10
0
-10
-20
-30
FREQUENCY SHIFT
(CM-1)

This behaviour is characteristic of the envelope maximum of a pure rotation band of a diatomic molecule.

A similar result was obtained in the high resolution spectra of xenon, which are shown in Figure 10. It was necessary in this case to use an 0.8 cm^{-1} slitwidth in order to obtain structure. Again, because of the rapid light loss with increasing resolution, it was not possible to go beyond the resolving power corresponding to 0.8 cm^{-1}; consequently, the peaks of the band structure (if any) could not be resolved as in the case of argon. However, the shoulders do shift toward the Rayleigh peak with decrease of xenon temperature just as the peaks did in the spectrum of argon. On going from a temperature of 300°K to 223°K at a constant pressure of 3123 mm Hg the frequency shift of the shoulders changes from ± 3.5 ± .5 cm^{-1} to approximately ± 3.0 ± .5 cm^{-1}.

Figure 11 is a plot of the logarithm of the frequency shifts of the band structure maxima or shoulders versus the logarithm of the absolute temperature for both argon and xenon. The slope of the curve for argon is 0.6 and for xenon, 0.5, in good agreement with the result expected if the band were a pure rotation band. For a pure rotation band Herzberg (Reference 37) gives the

Figure 10

High resolution Raman spectra of xenon at 3095 mm Hg pressure; 0.8 cm^{-1} slitwidth, 4880 Å laser line.

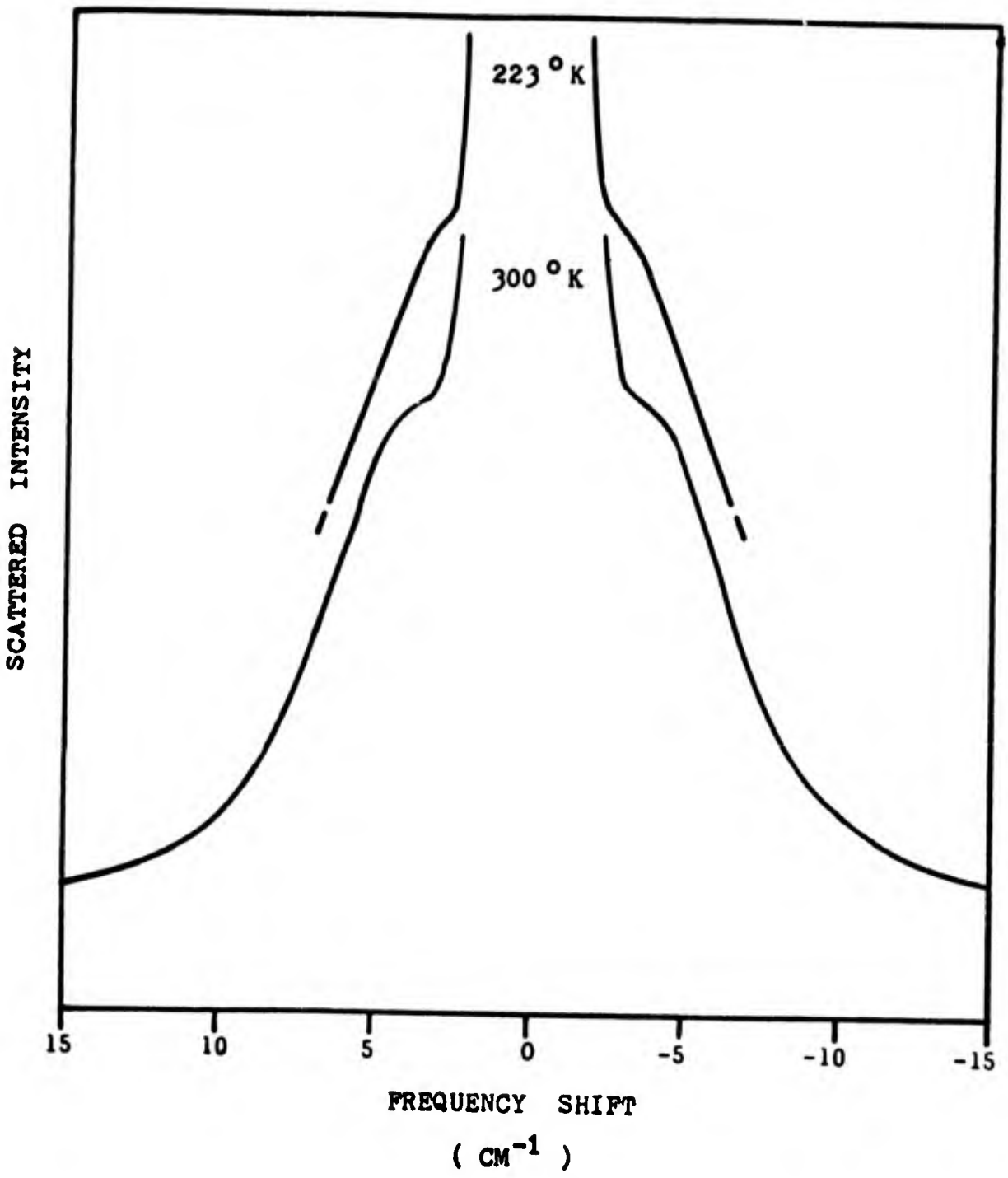
223 °K
300 °K
SCATTERED INTENSITY
15
10
5
0
-5
-10
-15
FREQUENCY SHIFT
(CM-1)

Figure 11

Shift of the band structure
with gas temperature.

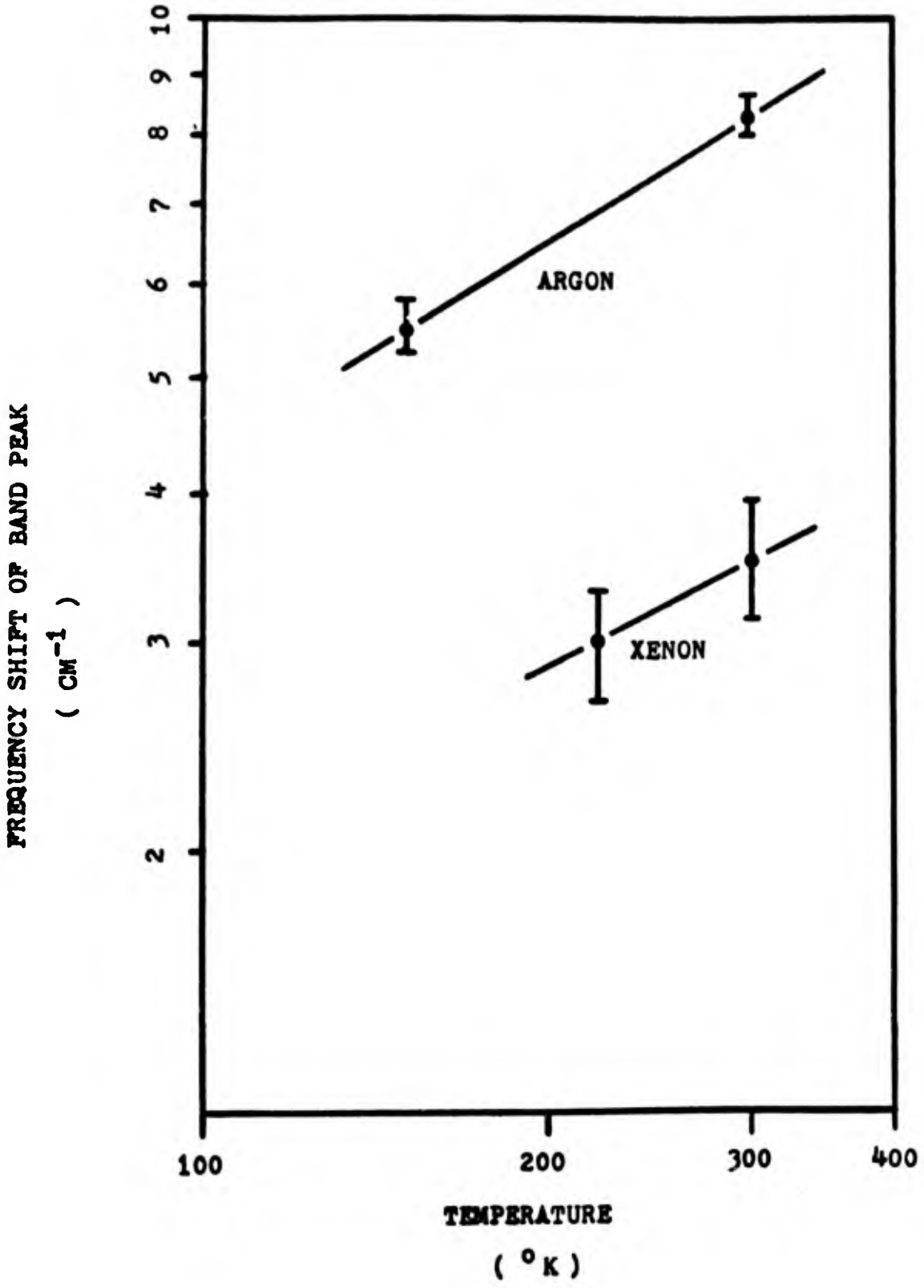
FREQUENCY SHIFT OF BAND PEAK
(CM^{-1})
2
3
4
5
6
7
8
9
10
ARGON
XENON
100
200
300
400
TEMPERATURE
(°K)

following formula for the rotational quantum number, J, corresponding to the maximum of the intensity of a pure rotation band:

$$J_{max} = \left(\frac{kT}{2Bhc}\right)^{1/2} - \frac{1}{2}$$

where k is Boltzmann's constant, T is absolute temperature, B is the rotational constant of the molecule, h is Planck's constant, and c is the velocity of light. The frequency shift $\Delta\nu$ in cm^{-1} for Raman scattering from a rigid rotator is given by (Reference 37)

$$|\Delta\nu| = 4B(J + 3/2)$$

where J is the rotational quantum number of the lower state. The above equations lead to an equation for the frequency shift of the band maximum given by

$$|\Delta\nu|_{max} = 4B\left(\left(\frac{kT}{2Bhc}\right)^{1/2} + 1\right)$$

Solving this equation for B, one obtains

$$B = \frac{1}{4}\left[|\Delta\nu|_{max} + \frac{kT}{hc} - \frac{kT}{hc}\left(1 + \frac{2hc}{kT}|\Delta\nu|_{max}\right)^{1/2}\right]$$

Substituting the values found for the frequency shifts at 300°K into this formula, one obtains the following results:

$$B = 0.04 \pm .008 \text{ cm}^{-1} \text{ for argon}$$

and

$$B = 0.009 \pm .003 \text{ cm}^{-1} \text{ for xenon}$$

Provided, of course, that the band structures are due to van der Waals dimers of argon and xenon respectively. Since the rotational constants are small,

$$\left(\frac{kT}{2Bhc}\right)^{1/2} > 1$$

and, therefore,

$$|\Delta\nu|_{max} \doteq 4B\left(\frac{kT}{2Bhc}\right)^{1/2}$$

Consequently,

$$\ln|\Delta\nu|_{max} \doteq \ln 4B + \frac{1}{2}\ln\frac{k}{2Bhc} + \frac{1}{2}\ln T$$

or

$$\frac{d(\ln|\Delta\nu|_{max})}{d(\ln T)} = 1/2$$

in agreement with the slopes of the curves shown in Figure 11.

In order to investigate further the temperature dependence and also the density dependence of the scattering, the signal intensity was increased by means of low resolution spectra taken with a 6 cm^{-1} slitwidth. The results for argon, at temperatures of 301°K, 222°K, and 157°K and a constant pressure of 3088 mm Hg are shown in Figure 12 and those for xenon at 301°K, 223°K, and 3095 mm Hg in Figure 13. A broad continuum monotonically increasing in intensity up to the Rayleigh line was observed for both argon and xenon. The intensity of this continuum increases with decreasing gas temperature and the ratio of the anti-Stokes intensity to the Stokes at a given Raman frequency shift is given by the Stokes factor (see Chapter III),

$$\frac{I_{AS}}{I_S} = \exp(-\ hc\ \Delta\nu/kT)$$

Figure 12

Low resolution Raman spectra of agron at 3088 mm Hg pressure; 6 cm^{-1} slitwidth, 4880 Å laser line.

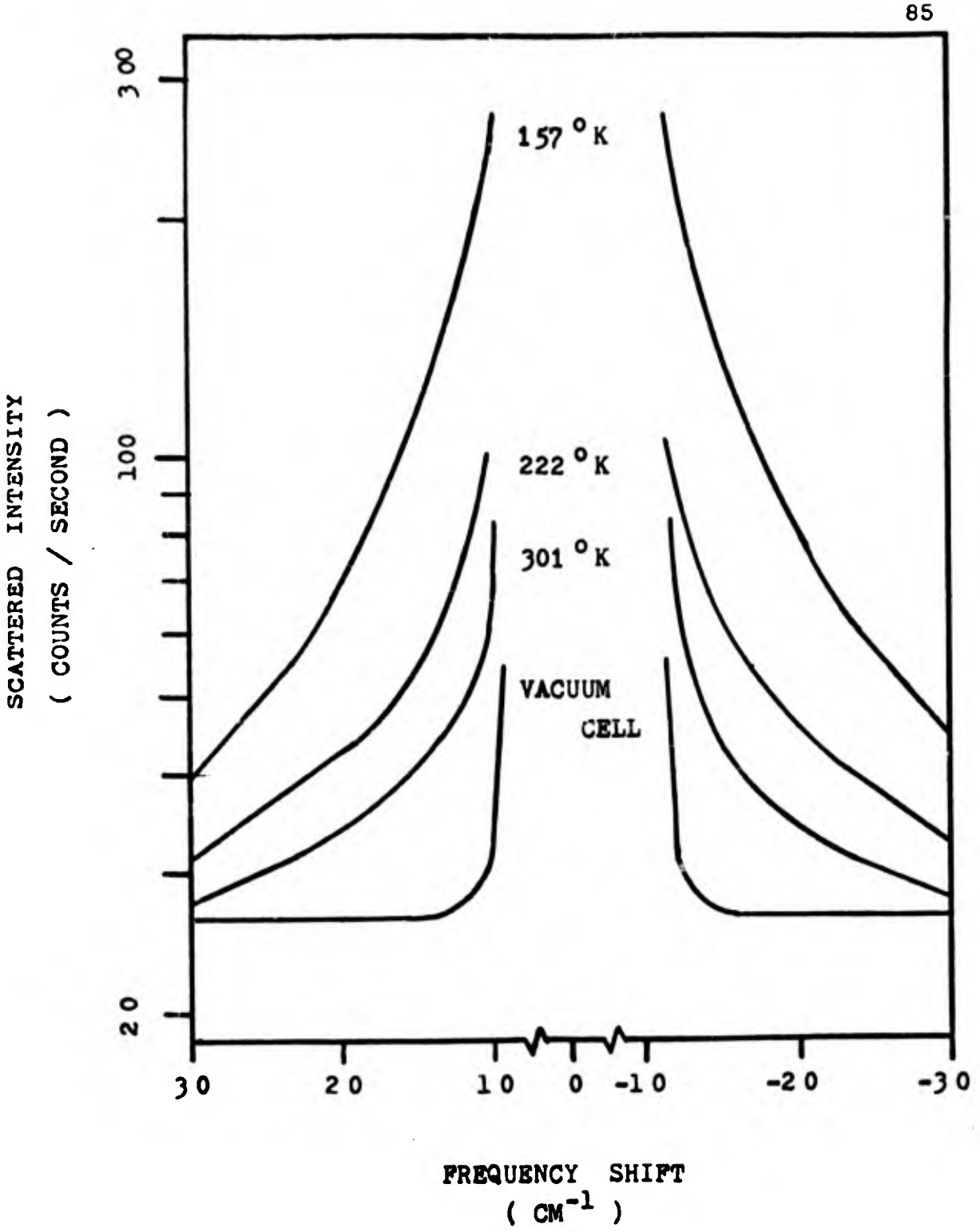
SCATTERED INTENSITY
(COUNTS / SECOND)
300
100
20
157 °K
222 °K
301 °K
VACUUM
CELL
30
20
10
0
-10
-20
-30
FREQUENCY SHIFT
(CM-1)

Figure 13

Low resolution Raman spectra of xenon at 3095 mm Hg pressure; 6 cm^{-1} slitwidth, 4880 Å laser line.

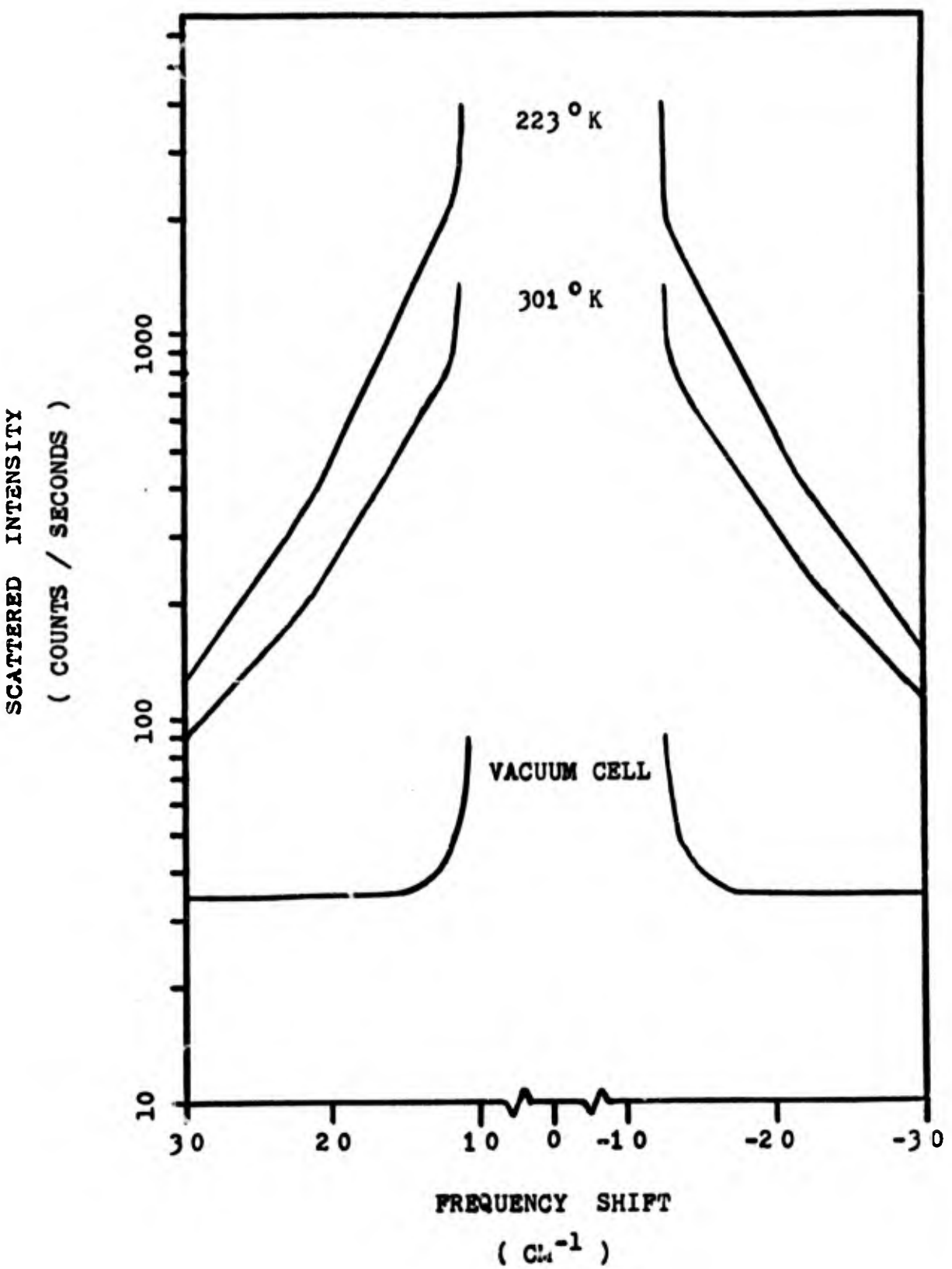
223 °K
301 °K
VACUUM CELL
1000
100
10
30
20
10
0
-10
-20
-30
SCATTERED INTENSITY
(COUNTS / SECONDS)
FREQUENCY SHIFT
(CM-1)

This result is illustrated in Figure 14 where the logarithm of the ratio of the anti-Stokes intensity to the Stokes intensity is plotted versus Raman frequency shift. The curves so obtained are straight lines with negative slope approximately given by the factor multiplying $\Delta\nu$ in the exponential of the above formula.

Returning to the low resolution spectra shown in Figures 12 and 13, one notes that the scattered intensity for xenon is much higher than that for argon. The scattered intensity plotted versus atomic polarizability is given in Figure 15. It is clearly seen that the Raman scattered intensity varies as the fourth power of the atomic polarizability of the parent gas. This is in distinct contrast to the variation of the Rayleigh scattered intensity, shown in Figure 16, which varies as the square of the atomic polarizability as expected (Reference 33). An attempt can be made to explain this result by a simple model. Suppose that, when two otherwise isolated noble gas atoms are brought close together, the action of the electronic charge distribution of one atom is to induce a dipolar charge distribution in that of the other atom. Thus, the charge distribution of one atom is a dipole with polarization $\bar{p}_1$ and that of the other atom also a dipole with a polarization $\bar{p}_2$. The polarization of the first atom due to the

Figure 14

Ratio of anti-Stokes to Stokes intensity of low resolution Raman spectra of argon and xenon as a function of frequency shift of the scattered light.

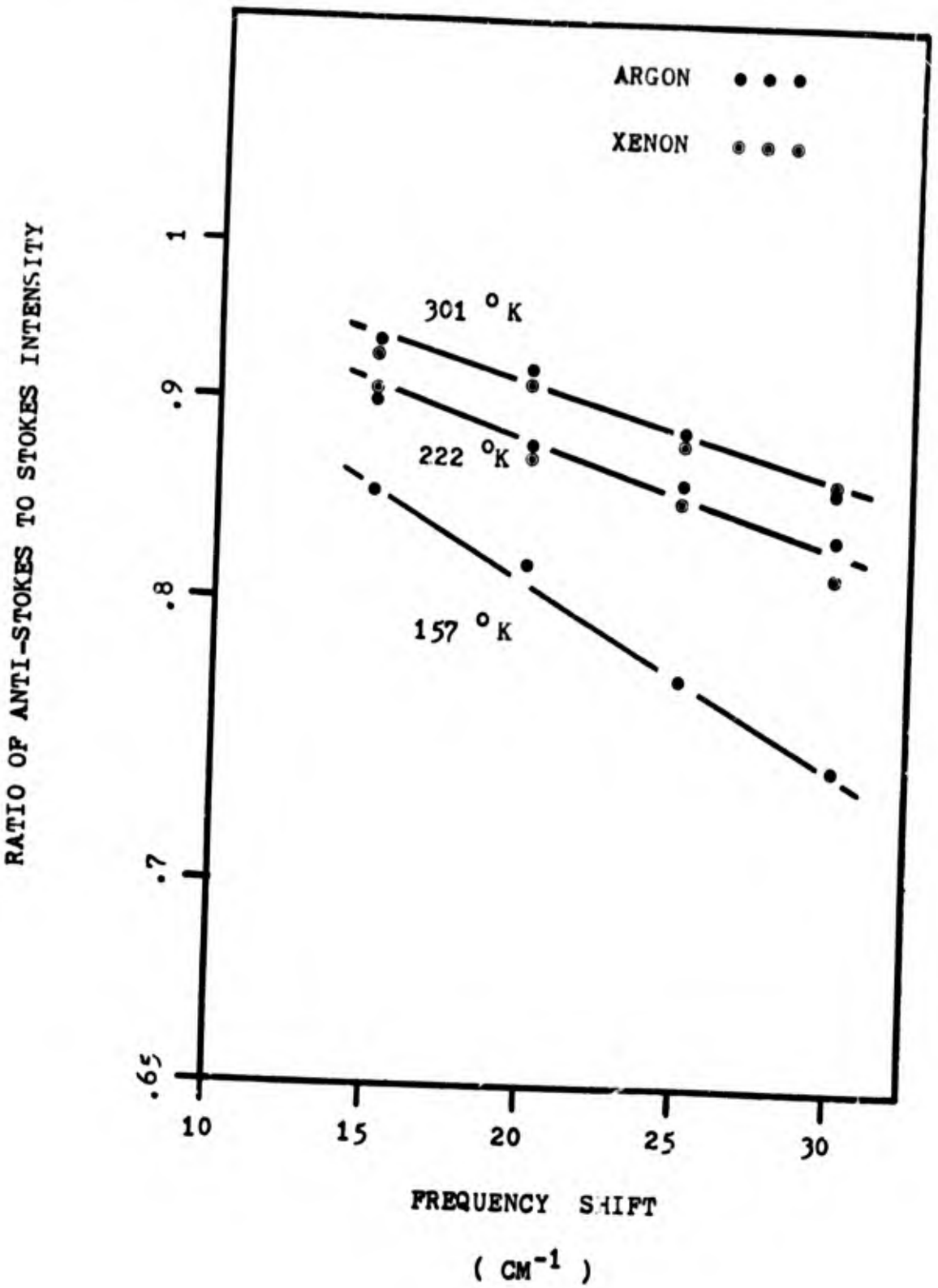
ARGON
XENON
301 °K
222 °K
157 °K
1
.9
.8
.7
.65
10
15
20
25
30
RATIO OP ANTI-STOKES TO STOKES INTENSITY
FREQUENCY SHIFT
(CM-1)

Figure 15

Raman intensity versus atomic polarizability of argon and xenon at constant frequency shift, temperature, and pressure.

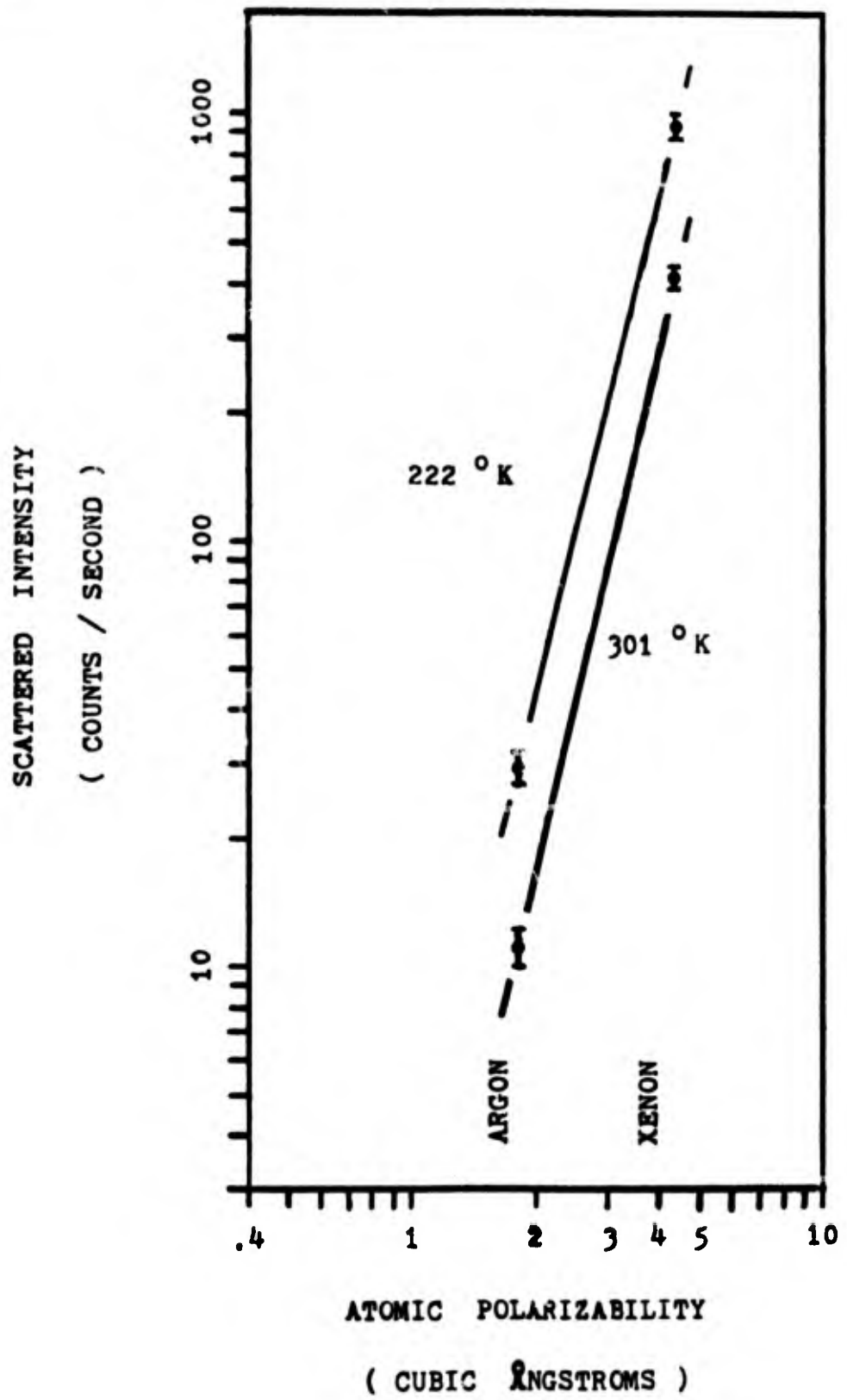
SCATTERED INTENSITY
(COUNTS / SECOND)
1000
100
10
222 °K
301 °K
ARGON
XENON
.4
1
2
3
4
5
10
ATOMIC POLARIZABILITY
(CUBIC ÅNGSTROMS)

Figure 16

Raleigh intensity versus atomic polarizability of argon and xenon at constant frequency shift, temperature, and pressure.

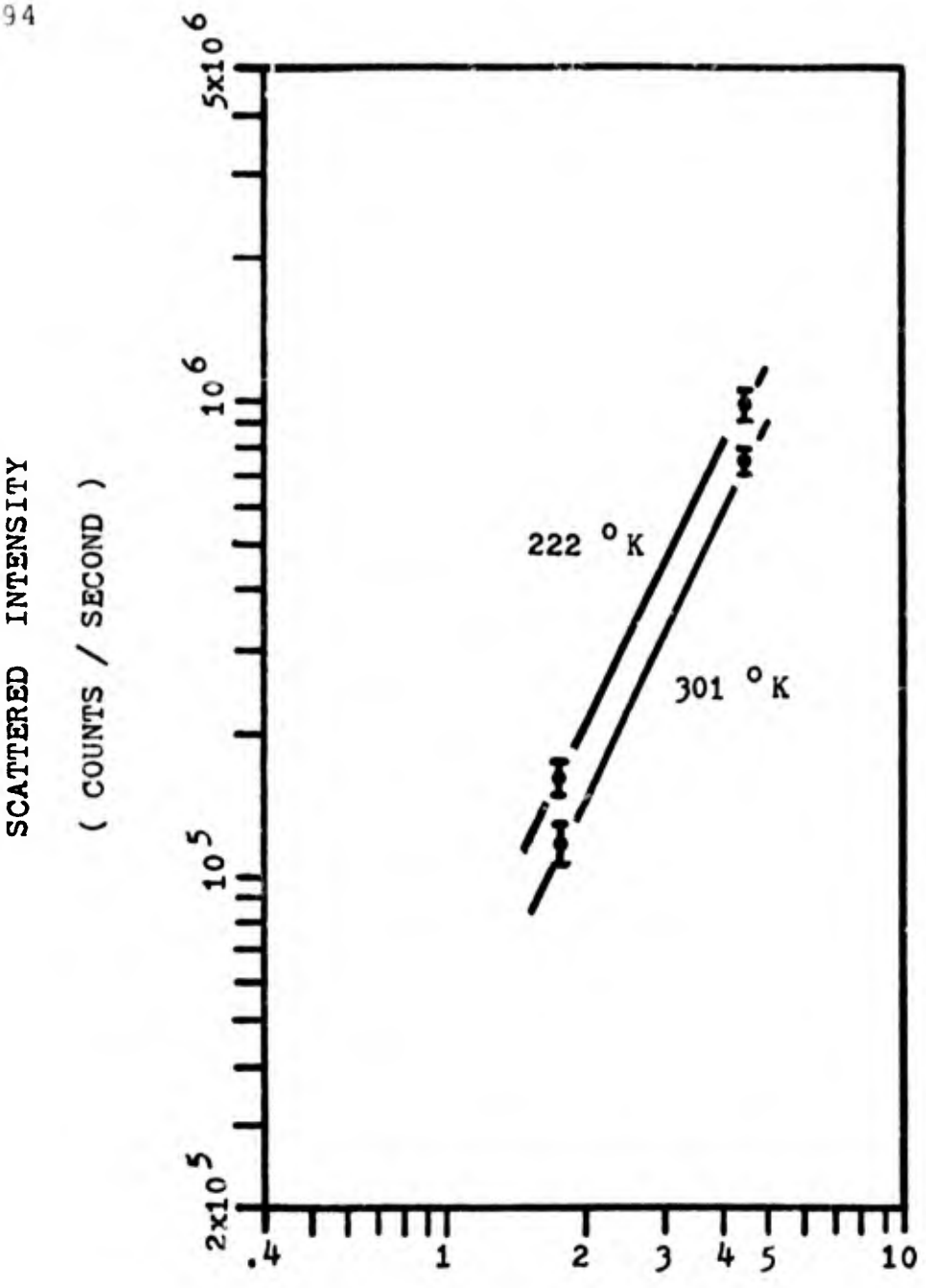
SCATTERED INTENSITY
(COUNTS / SECOND)
5x10^6
10^6
10^5
2x10^5
.4
1
2
3
4
5
10
222 °K
301 °K
ATOMIC POLARIZABILITY
(CUBIC ÅNGSTROMS)

electric field of the second atom is given by an internal electric field $\bar{E}_1$ where

$$\bar{p}_1 = \bar{\bar{\alpha}} \cdot \bar{E}_1$$

and where $\bar{\bar{\alpha}}$ is the atomic polarizability of the particular noble gas. Suppose further than an uniform electric field $\bar{E}$ is applied to the atoms, then the polarization now becomes

$$\bar{p}_1 = \bar{\bar{\alpha}} \cdot (\bar{E} + \bar{E}_1)$$

The net polarization of the two atoms by the applied field is

$$\bar{P} = \bar{p}_1 + \bar{p}_2$$

However, the charge distributions of each atom are not fixed and, as a consequence, one distribution collapses slightly while the other expands slightly under the action of $\bar{E}$. The result is that the magnitudes of $\bar{p}_1$ and $\bar{p}_2$ are not constant. The field $\bar{E}_1$ is given by (Reference 46)

$$\bar{E}_1 = - \left[\nabla_1 \nabla_2 \left(\frac{1}{r_{12}}\right)\right] \cdot \bar{p}_2$$

where r_{12} is the interatomic distance, ∇_i is the gradient operator with respect to center of mass coordinates of the i^{th} atom, and

$$\nabla_1 \nabla_2 \left(\frac{1}{r_{12}}\right) = \frac{1}{r_{12}^3} \left(\bar{\bar{1}} - \frac{3\bar{r}_{12}\,\bar{r}_{12}}{r_{12}^2}\right)$$

where $\bar{\bar{1}}$ is the identity dyadic. Let

$$\bar{\bar{G}}_{12} = \nabla_1 \nabla_2 \left(\frac{1}{r_{12}}\right)$$

Therefore,

$$\bar{p}_1 = \bar{\bar{\alpha}} \cdot \bar{E} - \bar{\bar{\alpha}} \cdot \bar{\bar{G}}_{12} \cdot \bar{p}_2$$

But

$$\bar{p}_2 = \bar{\bar{\alpha}} \cdot (\bar{E} + \bar{E}_2)$$

and

$$\bar{E}_2 = \bar{\bar{G}}_{21} \cdot \bar{p}_1$$

where $\bar{E}_2$ is the field at $\bar{p}_2$ due to $\bar{p}_1$. Consequently,

$$\bar{p}_1 = \bar{\bar{\alpha}} \cdot \bar{E} - \bar{\bar{\alpha}} \cdot \bar{\bar{G}}_{12} \cdot \bar{\bar{\alpha}} \cdot \bar{E}$$

$$+ \bar{\bar{\alpha}} \cdot \bar{\bar{G}}_{12} \cdot \bar{\bar{\alpha}} \cdot \bar{\bar{G}}_{21} \cdot \bar{p}_1$$

Applying the method of successive substitutions (Reference 47), one gets

$$\bar{p}_1 = (\bar{\bar{\alpha}} - \bar{\bar{\alpha}} \cdot \bar{\bar{G}}_{12} \cdot \bar{\bar{\alpha}}$$

$$+ \bar{\bar{\alpha}} \cdot \bar{\bar{G}}_{12} \cdot \bar{\bar{\alpha}} \cdot \bar{\bar{G}}_{21} \cdot \bar{\bar{\alpha}} - \ldots) \cdot \bar{E}$$

The same reasoning applies to $\bar{p}_2$ so that

$$\bar{P} = 2(\bar{\bar{\alpha}} - \bar{\bar{\alpha}} \cdot \bar{\bar{G}}_{12} \cdot \bar{\bar{\alpha}}$$

$$+ \bar{\bar{\alpha}} \cdot \bar{\bar{G}}_{12} \cdot \bar{\bar{\alpha}} \cdot \bar{\bar{G}}_{21} \cdot \bar{\bar{\alpha}} - \ldots) \cdot \bar{E}$$

Note that $\bar{\bar{G}}_{12} = \bar{\bar{G}}_{21}$ and that for an attractive force between the atoms $\bar{p}_1 = -\bar{p}_2$. The polarizability of the dimer is therefore,

$$\overline{\overline{\alpha}}_m = 2(\overline{\overline{\alpha}} - \overline{\overline{\alpha}} \cdot \overline{\overline{G}}_{12} \cdot \overline{\overline{\alpha}} + \overline{\overline{\alpha}} \cdot \overline{\overline{G}}_{12} \cdot \overline{\overline{\alpha}} \cdot \overline{\overline{G}}_{12} \cdot \overline{\overline{\alpha}} - \ldots)$$

Typical values of $\overline{\overline{\alpha}}$ and $\bar{r}_{12}$ are of the order of magnitude $|\overline{\overline{\alpha}}| = 10^{-24}$ to 10^{-23} cm^3 and $r_{12} = 10^{-8}$ to 10^{-7} cm, so that terms of higher order than the second in $\overline{\overline{\alpha}}_m$ may be neglected with the result that

$$\overline{\overline{\alpha}}_m = 2\left[\overline{\overline{\alpha}} - \overline{\overline{\alpha}} \cdot \frac{1}{r_{12}^3}\left(\overline{\overline{1}} - \frac{3\bar{r}_{12}\,\bar{r}_{12}}{r_{12}^2}\right) \cdot \overline{\overline{\alpha}}\right]$$

Two things can now be seen immediately: first, that, although $\overline{\overline{\alpha}}$ is isotropic, $\overline{\overline{\alpha}}_m$ is not and second, that the components of $\overline{\overline{\alpha}}_m$ perpendicular and parallel to the axis of the dimer are respectively

$$\overline{\overline{\alpha}}_{m\perp} = \left(\overline{\overline{\alpha}} - \frac{\overline{\overline{\alpha}} \cdot \overline{\overline{1}} \cdot \overline{\overline{\alpha}}}{r_{12}^3}\right)$$

and

$$\overline{\overline{\alpha}}_{m\parallel} = \left[\overline{\overline{\alpha}} - \overline{\overline{\alpha}} \cdot \frac{1}{r_{12}^3}\left(\overline{\overline{1}} - \frac{3\bar{r}_{12}\,\bar{r}_{12}}{r_{12}^2}\right) \cdot \overline{\overline{\alpha}}\right]$$

The anisotropy of $\overline{\overline{\alpha}}_m$ is given by (see Reference 18)

$$\overline{\overline{\gamma}}_m = \overline{\overline{\alpha}}_{m\parallel} - \overline{\overline{\alpha}}_{m\perp}$$

or

$$\overline{\overline{\gamma}}_m = \frac{3}{r_{12}^5}\left(\overline{\overline{\alpha}} \cdot \bar{r}_{12}\,\bar{r}_{12} \cdot \overline{\overline{\alpha}}\right)$$

$$= \frac{3}{r_{12}^3}\,\overline{\overline{\alpha}} \cdot \overline{\overline{\alpha}} = \frac{3\alpha^2}{r_{12}^3}$$

Now if it is assumed that the observed scattering is due to a pure rotation band of the van der Waals dimers, then the intensity I is proportional to

$$(\gamma_m')^2 = \left(\frac{\partial \overline{\overline{\gamma}}_m}{\partial Q}\right)^2$$

where Q is a generalized rotation coordinate (Reference 2). In this case, $\overline{\overline{\gamma}}_m$ must be strictly periodic with a period of π. If the scattering were due to vibration of the dimer, a periodic polarizability may not obtain because of the very strong possibility of anharmonic vibrations in van der Waals dimers (References 14 and 27). It seems reasonable to assume, therefore, that the spectra are due to rotation of dimers. Consequently,

$$\overline{\overline{\gamma}}_m = \overline{\overline{\gamma}}_{m0}\,\exp(2i\phi), \quad \gamma_m' = \overline{\overline{\gamma}}_m$$

where ϕ is the angle of rotation of the dimer. Finally we have

$$I = 9 I_0 \bar{\bar{\alpha}}^4 / r_{12}^6$$

or

$$I \propto \bar{\bar{\alpha}}^4$$

in agreement with the observations.

One of the most important results of the low resolution data is obtained by plotting the slope of the logarithm of the intensity with respect to frequency shift (obtained from the curves of Figures 12 and 13) versus temperature. The result shown in Figure 17 demonstrates that the slope varies as the inverse absolute temperature. This result agrees with neither the theories of Birnbaum and McTague (Reference 18) nor Gersten (Reference 31), nor Van Kranendonk (Reference 32), nor any of the older theories of scattering in atomic gases (References 36 and 19), all of which predict that the linewidth of the scattering should vary as the reciprocal of the velocity of the atom or, in other words, as the reciprocal of the square root of the absolute temperature. Further, if the same slopes

Figure 17

Slope of the logarithm of the Raman intensity with respect to frequency shift as a function of gas temperature for argon and xenon at constant pressure and for frequency shift ranges of 14 cm^{-1} to 22 cm^{-1} and 22 cm^{-1} to 30 cm^{-1}.

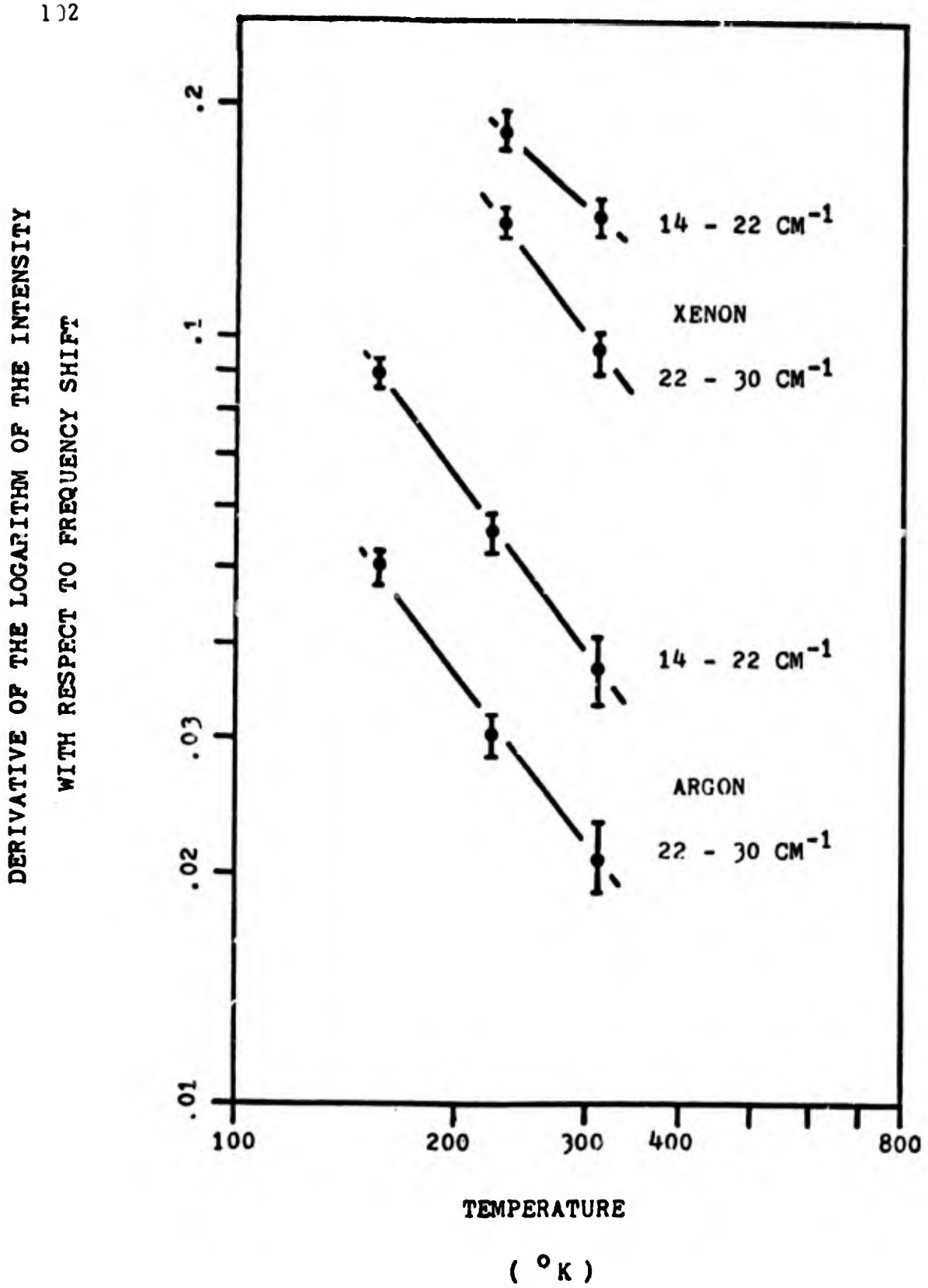
DERIVATIVE OF THE LOGARITHM OF THE INTENSITY
WITH RESPECT TO FREQUENCY SHIFT
.2
.1
.03
.02
.01
14 - 22 CM-1
XENON
22 - 30 CM-1
14 - 22 CM-1
ARGON
22 - 30 CM-1
100
200
300
400
800
TEMPERATURE
(°K)

are plotted versus the rotational constants derived from the high resolution data as illustrated in Figure 18, the result is that the slopes vary as the reciprocal of the first power of the rotational constant. In contrast, such a plot versus atomic weight gives curves with slopes of +1.25 to +1.30. It appears that the dependence of the slope on rotational constant is by far the most natural and satisfying.

Both of these things may easily be understood if it is assumed that the scattering is a result of a pure rotation band of a van der Waals dimer. It was shown in Chapter III that the slope of the logarithm of the intensity verus frequency shift of a var der Waals dimer is given by

$$\frac{d}{d|\Delta\nu|}\left(\mathrm{Ln}I/I_0\right) = -\,2hc|\Delta\nu|/kTB$$

This equation thus exhibits the observed dependence of the slope on B and T.

Depolarization ratios were also measured at low resolution. The Raman scattering was observed at right angles to the direction of the laser beam and the electric vector of the laser light. The laser light was polarized

Figure 18

Slope of the logarithm of the Raman intensity with respect to frequency shift versus the derived rotational constants of argon and xenon at constant pressure and temperature and for frequency shift ranges of 14 cm^{-1} to 22 cm^{-1}, and 22 cm^{-1} to 30 cm^{-1}.

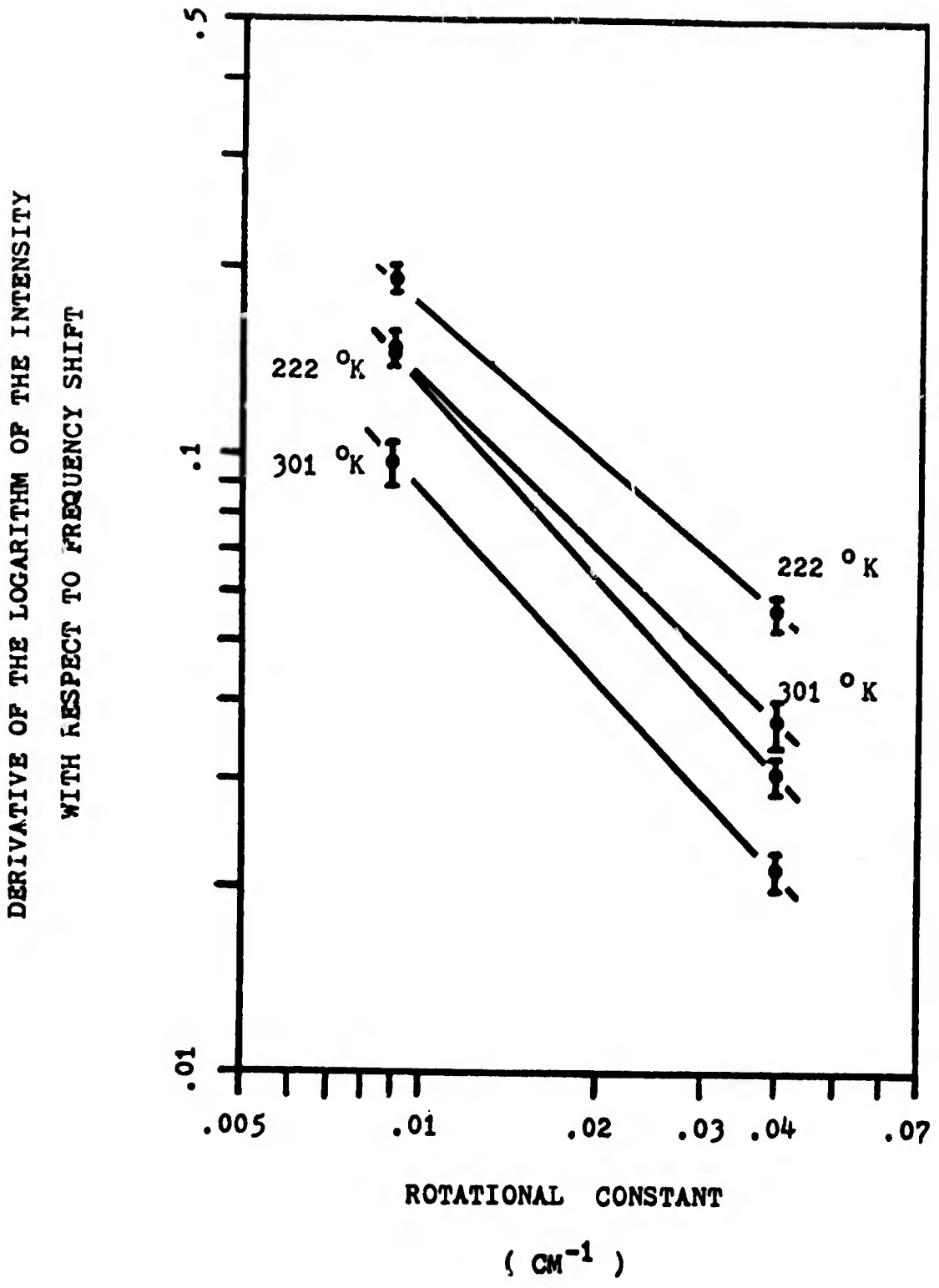
DERIVATIVE OF THE LOGARITHM OF THE INTENSITY
WITH RESPECT TO FREQUENCY SHIFT
.5
.1
.01
222 °K
301 °K
222 °K
301 °K
.005
.01
.02
.03
.04
.07
ROTATIONAL CONSTANT
(CM-1)

with the electric vector in the horizontal plane and the laser beam was directed vertically upward. The correct formula for the observed depolarization ratio ρ is given by Gibson and Hendra (Reference 48) as

$$\rho = \frac{3\bar{\bar{\gamma}}^2 + 3d_z\bar{\bar{\gamma}}^2 + 8\bar{\bar{\alpha}}^2}{45\bar{\bar{\alpha}}^2 + 4\bar{\bar{\gamma}}^2 + 3d_x\bar{\bar{\gamma}}^2}$$

where d_z is the correction factor given by Stenhouse (see Reference 48) for divergence of the collection beam in the vertical direction and d_x, that for divergence in the direction of the electric vector of the laser light and δ is the correction factor investigated by Baxter (Reference 49) for passage of skew rays of the light analyzed against through the polarizer. For a pure rotation band the isotropic component, $\bar{\bar{\alpha}}$, of the polarizability tensor does not contribute to the scattering (the scattered light is completely depolarized) and for the instrument used in these studies d_x and d_z were measured to be $d_x = .05$ and $d_z = .03$. Hence, with the use of the instrument in this laboratory the depolarization ratio is given by

$$\rho = \frac{3\bar{\bar{\gamma}}^2 + .09\bar{\bar{\gamma}}^2}{4\bar{\bar{\gamma}}^2 + .15\bar{\bar{\gamma}}^2} = .744$$

For argon the measured value for ρ (both Stokes and anti-Stokes) is

$$\rho = 0.74 \pm .05$$

and for xenon

$$\rho = 0.75 \pm .05$$

indicating that the observed scattering is completely depolarized.

A further indication that the scattering is due neither to impurities nor stray light is afforded by the fact that the intensity depends on the square of the gas density. The density dependence is shown in Figures 19 and 20 for argon and xenon, respectively. On the other hand, the Rayleigh scattering was found to vary linearly with density. In the case of xenon the data, which were taken at 223°K, exhibit a change from a square law dependence on density to a cubic variation above a gas density of 4.5 amagats. It appears that a triatomic process is occurring at these higher densities and low temperatures--perhaps the formation of trimers. Further investigation

Figure 19

Raman intensity as a function of argon density at 16 cm^{-1} frequency shift; 6 cm^{-1} slitwidth, 4880 Å laser line.

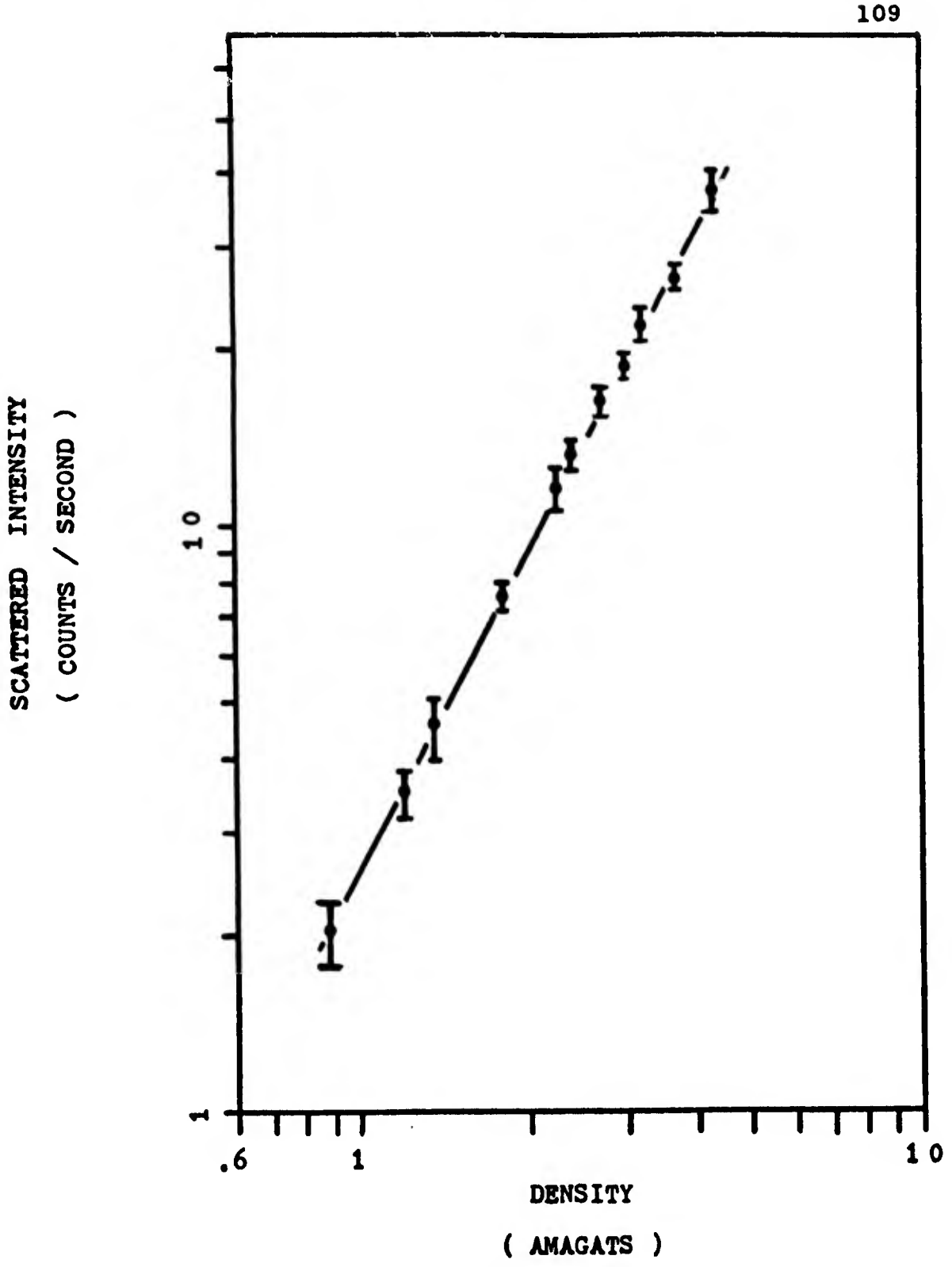
SCATTERED INTENSITY
(COUNTS / SECOND)
10
1
.6
1
10
DENSITY
(AMAGATS)

Figure 20

Raman intensity as a function of xenon density at 16 cm^{-1} frequency shift and 223 °K; 6 cm^{-1} slitwidth, 4880 Å laser line.

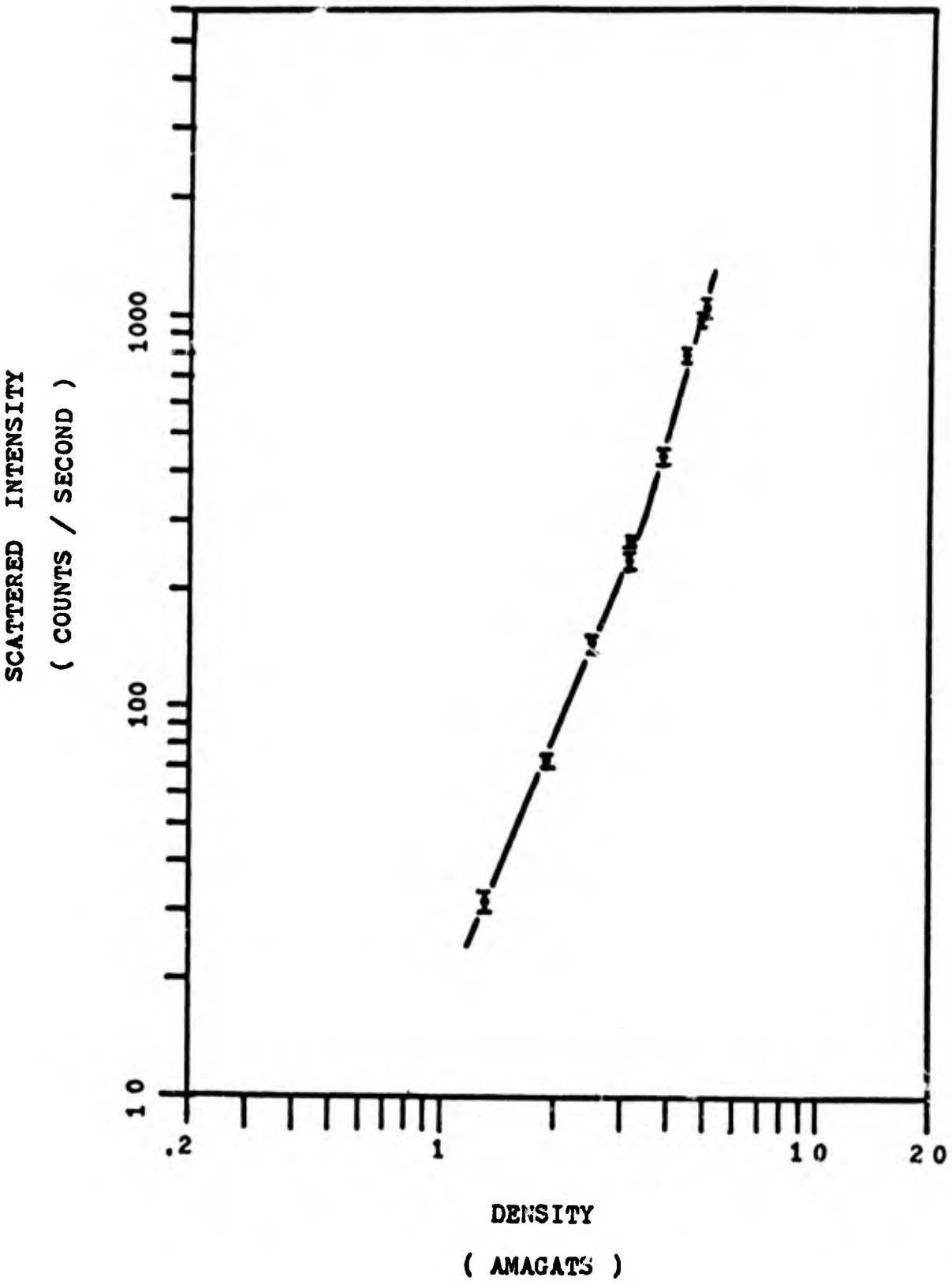
SCATTERED INTENSITY
(COUNTS / SECOND)
1000
100
10
.2
1
10
20
DENSITY
(AMAGATS)

of this process would require rebuilding the sample cell for high pressures. The density dependence of the intensity is consistent with scattering by van der Waals dimers.

Finally, the dependence of the scattered intensity on the gas temperature was investigated and it was found that the intensity is proportional to $T^{-7/2}$ at constant gas pressure in both argon and xenon. The results are plotted in Figure 21. The temperature variation of the intensity shown there is in excellent agreement, therefore, with the predictions of Stogryn and Hirschfelder for van der Waals dimers. In addition, this result agrees well with the mass spectrometer measurements of Leckenby and Robbins on argon and xenon in which the same temperature dependence was observed for the number density of dimers.

On the other hand, no scattering that could be attributed to a vibration band of the dimers was found in the range of frequency shifts of $\pm$ 50 cm^{-1} about the Rayleigh line for both argon and xenon. In the low resolution spectra of argon, a small bulge of a few counts per second in the spectra at low temperatures was observed at $\pm$ 25 cm^{-1} which could have been the vibration line at

Figure 21

Raman intensity as a function of temperature at 3090 mm Hg and 16 cm^{-1} frequency shift; 6 cm^{-1} slit-width, 4880 Å laser line.

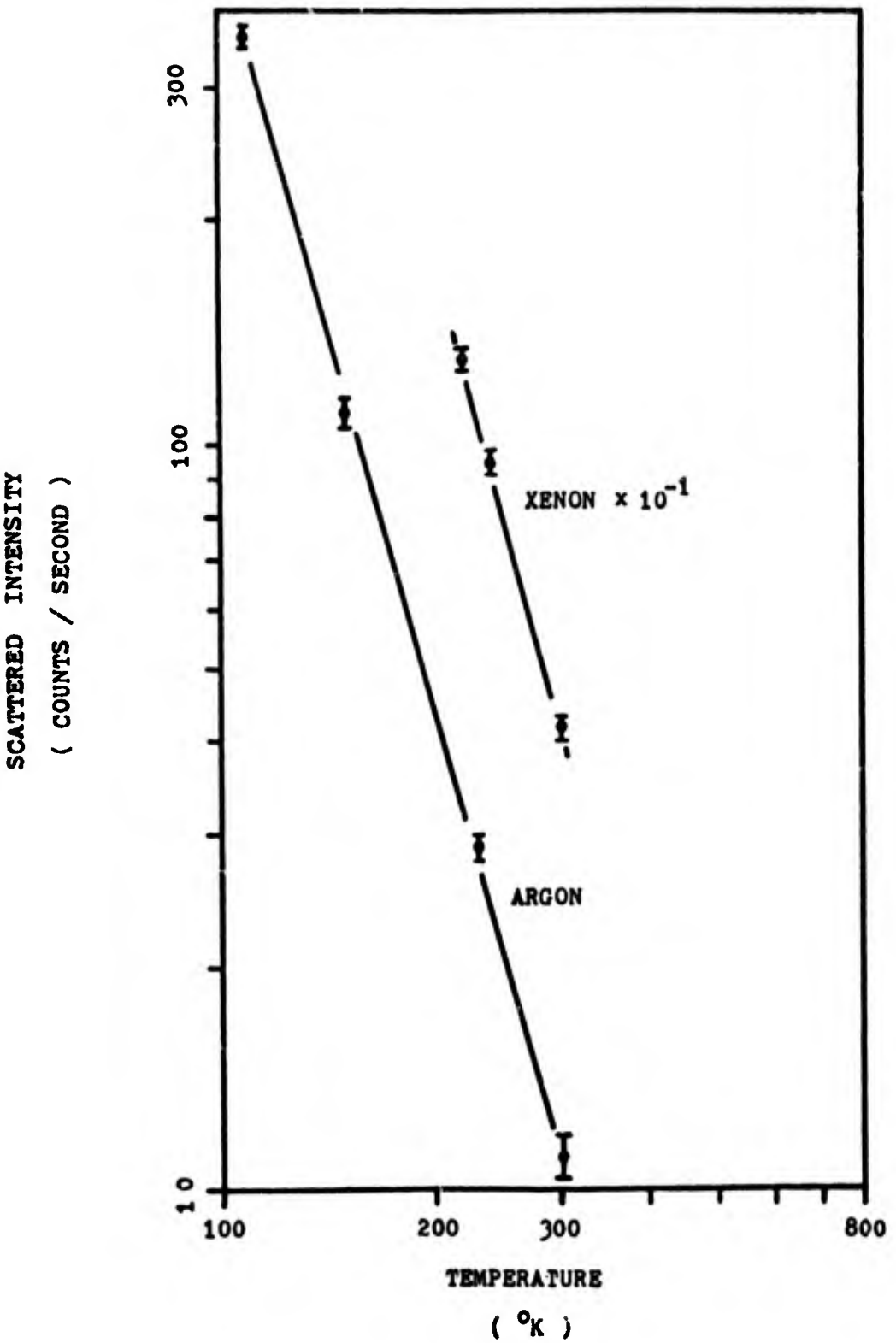
SCATTERED INTENSITY
(COUNTS / SECOND)
300
100
10
XENON x 10^{-1}
ARGON
100
200
300
800
TEMPERATURE
(°K)

25 cm^{-1} reported by Tanaka and Yoshino in argon (Reference 27) but which otherwise is of doubtful significance. The best that can be said is that the data reported here neither confirms nor negates the presence of vibration bands. This result is not totally inconsistent with the interpretation of dimers as the source of scattering for at least two reasons. First, it is a general consequence of the Raman spectroscopy of gases of normal molecules such as N_2 and O_2 that the pure rotation band has much greater intensity than any of the vibration bands (see Stoicheff Reference 50). For example, with the present instrument the observed intensities of vibration bands in N_2 and O_2 are less than one-tenth the intensities of the corresponding pure rotation bands. Stoicheff (Reference 50) reports that exposure times of a few hours are required for pure rotation spectra while exposure times of 20 to 100 hours are required for vibration bands. Consequently, because of the very low intensities observed in this work, the vibration bands should be undetected. Second, there is the distinct possibility that the metastable dimers exist in much greater concentration than the stable dimers. Most of the metastable dimers very likely do not have vibrational levels, so that the absence of vibration bands in the spectra may be accounted for in this way. It has

been proposed that the association of two atoms proceeds in two stages (References 51 and 52). In the first step a metastable or resonant state of the dimer is formed in a collision of two atoms. If a third atom then collides with this complex, it can take away excess energy and a stable dimer is left. Indeed, if this process of two successive two-body collisions is more frequent than the formation of stable dimers by the simultaneous collision of three atoms, the concentration of metastable dimers should be greater than that of the stable dimers.

Because of the high intensity of the focused laser beam, it might well be supposed that the laser intensity influences the population of dimers, particularly if the laser heats the gas appreciably. Accordingly, the scattered intensity was observed as the laser power was increased from the threshold up to full power. The results of this investigation are shown in Figure 22 from which it can be seen that there is no measurable effect--the intensity increasing as the square of the gas pressure at constant laser power and linearly with laser power at constant pressure.

Figure 22

Raman intensity as a function of laser power for argon at 300 °K, 6 cm^{-1} slitwidth, 4880 Å laser line.

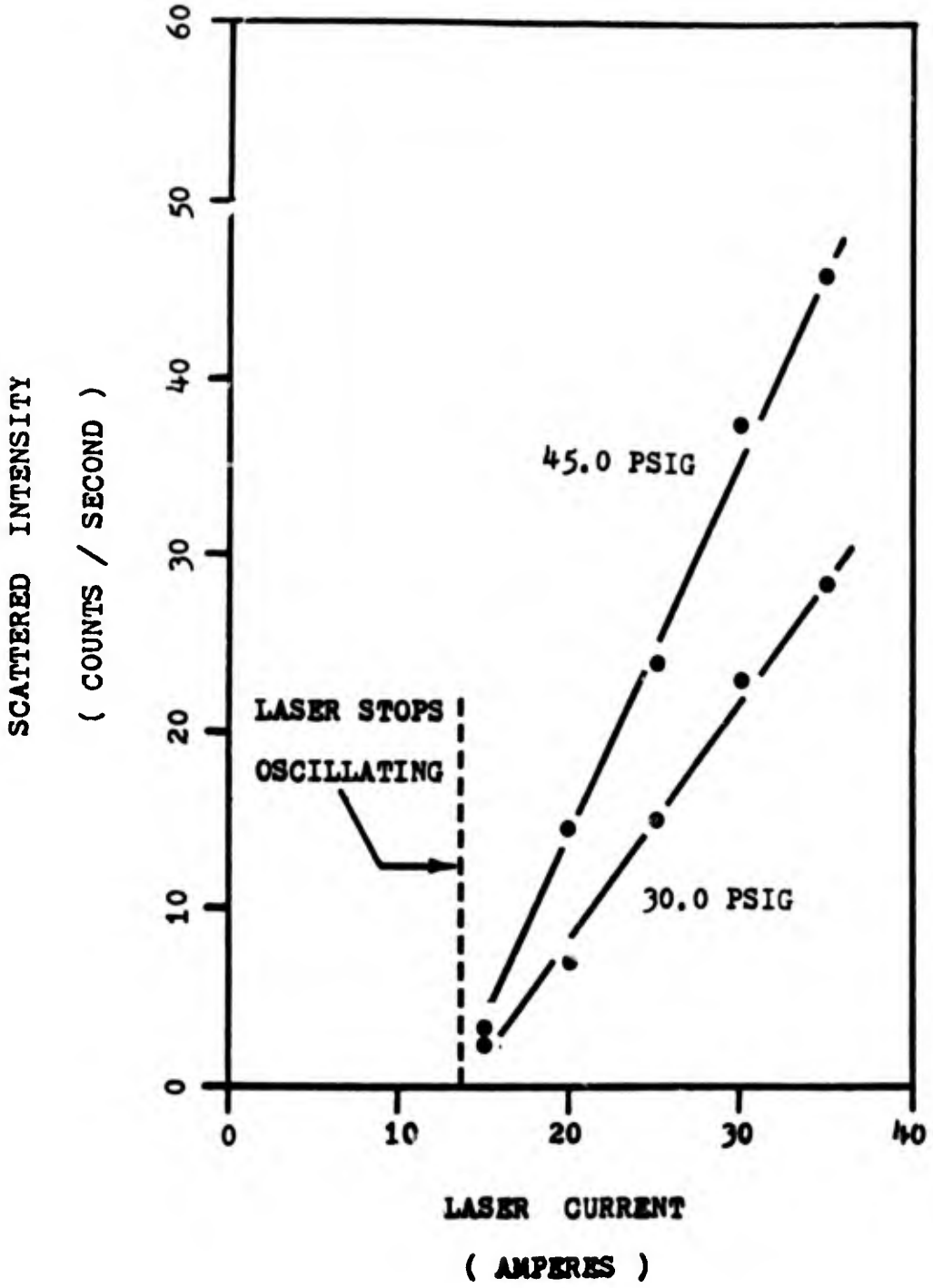
SCATTERED INTENSITY
(COUNTS / SECOND)
0
10
20
30
40
50
60
0
10
20
30
40
LASER CURRENT
(AMPERES)
LASER STOPS
OSCILLATING
45.0 PSIG
30.0 PSIG

C H A P T E R V I

CONCLUSIONS

On the one hand, the results presented here for Raman scattering by argon agree with the results obtained by previous workers in that the scattering is completely depolarized, varies as the square of the density, and the ratio of the anti-Stokes to Stokes intensity is given by a Boltzmann factor. On the other hand, the variation of linewidth observed in this work with temperature and variation of intensity with temperature do not agree with that predicted by present theories of light scattering from noble gases. In distinguishing the mechanism of scattering, the variation of linewidth with temperature is crucial, for it is clear that if the scattering is a result of unbound collision pairs the linewidth must vary as the duration time of collision (i.e., as $T^{-1/2}$ and directly as the reduced mass), while if the scattering is due to molecules, the linewidth must vary according to quantum mechanics as T^{-1} and inversely with the rotational constant. In addition, at high resolution, band structures were observed which resembled unresolved pure rotation

bands especially in their behaviour as the temperature is lowered. In spite of the fact that it was not possible to resolve rotation lines and that nothing was detected which could be reliably called a vibration band, the observed scattering strongly appears to be Raman scattering by van der Waals dimers.

All the data reported here is consistent with this interpretation of scattering from van der Waals dimers. Moreover, the complete depolarization of the scattered light seems best explained by rotation of the dimers. The absence of measurable vibration is due to either the inherent low intensity of vibration bands in Raman spectra of gases or the possibility of large numbers of metastable dimers of high angular momentum. In the present experiment both metastable and stable dimers should be detected. The number of vibrational levels decreases with increasing angular momentum as shown by Buluggiu and Foglia (Reference 53), who report the number of vibrational levels for rare gas dimers calculated from theory. For argon, only one vibrational level exists for values of the angular momentum quantum number ℓ given by

$$7 \leq \ell \leq 22$$

and for xenon, only one level exists for

$$23 \leq \ell \leq 65.$$

The majority of high angular momentum states, at least in the case of argon, would exhibit, therefore, no vibrational lines. Stogryn and Hirschfelder (Reference 4) exhibit a series of effective potential curves for the Lennard-Jones (6-12) potential in which the one given by

$$\frac{\hbar^2 \ell(\ell + 1)}{2m\epsilon\sigma^2} = 1.3261$$

appears to be the lowest metastable state curve. The lowest metastable state corresponds to $\ell = 44$ for argon and $\ell = 75$ for xenon. It seems reasonable to conclude that the metastable states would have no more than one vibrational level. If the stable dimers are formed through the metastable dimers as intermediate steps, then it would seem necessary that the metastable dimers should exist in greater concentration than the stable dimers. Since the shape of the spectra does not appear to depend on the gas density, the linewidth does not depend on the time between collisions in the gas. This behaviour is consistent with

scattering by metastable dimers, particularly those with high angular momentum and, therefore, with lifetimes less than the time between collisions in the gas.

The values of the interatomic distances derived from the rotational constants obtained from the spectra are

$r_e = 4.57 \pm .5$ Å for argon and

$r_e = 5.35 \pm .2$ Å for xenon.

These values compare with the ground state equilibrium radii given by Hirschfelder (Reference 54) as

$r_e = 3.82$ Å for argon and

$r_e = 4.60$ Å for xenon.

The minimum value of the interatomic distance corresponding to the centrifugal hump in the effective interatomic potential is the interatomic distance corresponding to the critical energy as defined by Hirschfelder (locus cit.) and given by

$r_c = 5.97$ Å for argon and

$r_c = 7.19$ Å for xenon.

Accordingly the measured interatomic distances can be seen to be reasonable values consistent with the anharmonicity of the Lennard-Jones potential.

The experimental method of Raman spectroscopy used in this work is an effective and simple way to determine the molecular properties of complexes due to the van der Waals forces in gases. The basis has, perhaps, been laid for the study not only of the stable van der Waals molecules, but also the metastable molecules.

LIST OF REFERENCES

1. Noble-Gas Chemistry, John H. Holloway, Methuen and Co. Ltd., London (1968), p. 3 et seq.

2. The Dynamical Theory of Gases, J. H. Jeans, Cambridge University Press, London (1925), p. 193 et seq.

3. Kinetic Theory of Liquids, J. Frenkel, Oxford University Press (1946).

4. Daniel E. Stogryn and Joseph O. Hirschfelder, Journal of Chemical Physics 31, 1531 (1959).

5. Daniel E. Stogryn and Joseph O. Hirschfelder, Journal of Chemical Physics 31, 1545 (1959).

6. Hai Vu and Boris Vodar, Zeitschrift für Electrochemie 64, 756 (1969).

7. A. Watanabe and H. L. Welsh, Physical Review Letters 13, 810 (1965).

8. P. E. Leckenby, E. J. Robbins, and P. A. Trevalion, Proceedings of the Royal Society (London) A280, 409 (1964).

9. R. E. Leckenby and E. J. Robbins, Nature 207, 1253 (1965).

10. R. E. Leckenby and E. J. Robbins, Proceedings of the Royal Society (London) A·291, 389 (1966).

11. A. Watanabe and H. L. Welsh, Canadian Journal of Physics 43, 818 (1965).

12. A. Kudian, H. L. Welsh, and A. Watanabe, Journal of Chemical Physics 43, 3397 (1965).

13. Elizabeth J. Allin, A. D. May, B. F. Stoicheff, J. C. Stryland, and H. L. Welsh, Applied Optics 6, 1597 (1967).

14. A. R. W. McKellar and H. L. Welsh, Journal of Chemical Physics 55, 595 (1971).

15. E. A. Ogryzlo and B. C. Sanctuary, Journal of Physical Chemistry 69, 4422 (1965).

16. Thomas A. Milne and Frank T. Greene, Journal of Chemical Physics 47, 4095 (1967).

17. J. P. McTague and George Birnbaum, Physical Review Letters 21, 661 (1968).

18. J. P. McTague and George Birnbaum, Physical Review A3, 1376 (1971).

19. Harold B. Levine and George Birnbaum, Physical Review Letters 20, 439 (1968).

20. Shardanand, Physical Review 160, 67 (1967).

21. Shardanand, Journal of Quantitative Spectroscopy and Radiative Transfer 8, 1373 (1968).

22. Y. Tanaka and K. Yoshino, Journal of Chemical Physics 50, 3087 (1969).

23. T. H. Lyman, Astrophysics Journal 60, 1 (1924).

24. L. A. Sommer, Proceedings of the National Academy of Science (U.S.) 13, 213 (1927).

25. J. J. Hopfield, Astrophysics Journal 72, 133 (1930).

26. J. L. Nickerson, Physical Review 47, 707 (1935).

27. Y. Tanaka and K. Yoshino, Journal of Chemical Physics 53, 2012 (1970).

28. Y. Tanaka, Journal of the Optical Society of America 45, 710 (1955).

29. P. G. Wilkinson and Y. Tanaka, Journal of the Optical Society of America 45, 344 (1955).

30. J. I. Gersten, R. E. Slusher, and C. M. Surko, Physical Review Letters 25, 1739 (1970).

31. Joel I. Gersten, Physical Review A4, 98 (1971).

32. J. Courtenay Lewis and J. van Kranendonk, Physical Review Letters 24, 802 (1970).

33. G. Placzek, The Rayleigh and Raman Scattering, UCRL-Trans-526 (L), U.S. Atomic Energy Commission (1962).

34. G. W. Chantry, The Raman Effect, Volume I, Principles. A. Anderson, Editor, Marcel Dekker Inc., New York (1971), Chapter 2, p. 49.

35. T. J. Greytek and G. B. Benedek, Physical Review Letters 17, 179 (1966).

36. O. Theimer and R. Paul, Journal of Chemical Physics 42, 2508 (1965).

37. Gerhard Herzberg, Molecular Spectra and Molecular Structure, Volume I, Spectra of Diatomic Molecules, D. Van Nostrand Co., Inc., Princeton, New Jersey (1950).

38. V. L. Chupp and P. C. Grantz, Applied Optics 8, 925 (1969).

39. Ralph Stair, Russell G. Johnston, and E. W. Halbach, Journal of Research of the National Bureau of Standards, No. 4, 291 (1960).

40. W. B. Bridges and Arthur N. Chester, Applied Optics 4, 573, (1965).

41. A. Weber and E. A. McGinnis, Journal of Molecular Spectroscopy 4, 195 (1960).

42. Howard H. Claassen, Henry Selig, and Jacob Shamir, Applied Spectroscopy 23, 8 (1969).

43. J. Brandmuller, K. Burchardi, H. Hacker, and H. W. Schrotter, Zeitschrift für Physik 22, 177 (1967).

44. Robert C. Weast, Editor, Handbook of Chemistry and Physics, 51st Ed., The Chemical Rubber Company, Cleveland (1970), p. E-115.

45. Leonard R. Ingersoll, Otto J. Zobel, Alfred C. Ingersoll, Heat Conduction with Engineering, Geological, and Other Applications. University of Wisconsin Press, Madison, Wisconsin (1954).

46. John David Jackson, Classical Electrodynamics, John Wiley and Sons, New York (1966), p. 105.

47. R. Courant and D. Hilbert, Methods of Mathematical Physics, Volume I, Interscience, Inc., New York (1966), pp. 17-23.

48. T. R. Gilson and P. J. Hendra, Laser Raman Spectroscopy, Wiley-Interscience, London (1970).

49. Lincoln Baxter, Journal of the Optical Society of America 46, 435 (1956).

50. B. P. Stoicheff, Advances in Spectroscopy, H. W. Thompson, Ed., Volume I, Interscience, New York (1959), p. 91.

51. R. D. Levine, Journal of Chemical Physics 46, 331 (1967).

52. R. E. Roberts, R. B. Bernstein, and C. F. Curtiss, Journal of Chemical Physics 50, 5163 (1969).

53. E. Buluggiu and C. Foglia, Il Nuono Cimento 43, 197 (1966).

54. Joseph O. Hirschfelder, Charles F. Curtiss, and R. Byron Bird, Molecular Theory of Gases and Liquids, John Wiley and Sons, Inc., New York (1964), p. 165.